Fragmentation of the Adriatic Promontory: New Chronological Constraints From Neogene Shortening Rates Across the Southern Alps (NE Italy)

Adrien Moulin, Lucilla Benedetti

Fragmentation of the Adriatic promontory : new chronological constraints from Neogene shortening rates across the Southern Alps (NE Italy)

Adrien Moulin[1,2]* and Lucilla Benedetti[1]

[1]Aix Marseille Univ, CNRS, IRD, INRA, Coll France, CEREGE, Aix-en-Provence, France

[2]Now at Department of Earth & Planetary Sciences, University of California, Davis, California, USA

Key-points

Folded alluvial surfaces and balanced cross-section constrain post-LGM and Neogene shortening-rates

Decrease in shortening-rate and change in compression direction are inferred at 1-2 Ma

Kinematic reorganization is best explained by a shift from Nubia-driven to Adria-driven convergence

Abstract

The eastern Southern Alps are located at the northern tip of the Adria microplate, which imposes 2.0-2.5-mm/yr of N-S-convergence relative to stable Eurasia. We map surface evidence of recent folding/faulting in this area from a 5-m-DEM. In the eastern part of the belt, observations reveal a 30-km-wide zone of active folding composed of at least five growing anticlines. The most recent ones warped the post-glacial alluvial surface by <10m. Combining these findings with published geological and geophysical data allows us to infer that active thrusting occurs along a single deeply rooted thrust, which accommodates the indentation of the Adriatic crust. Resolving the observed pattern of uplift on the inferred fault geometry indicates that NNE-SSW-shortening across the eastern Southern Alps has occurred at a rate of about 1.5 mm/yr over the post-glacial period. On the other hand, a balanced cross-section for the eastern Southern Alps at the scale of the upper crust constrains a minimum of 43 km of finite shortening over the last 14Ma, yielding a shortening-rate of about 3 mm/yr, which is two times higher than the post-glacial shortening-rate. This decrease in the shortening-rate is associated to the Pleistocene activation of new thrusts that is compatible with a change in the direction of compression. The inferred local change in the kinematics of thrusting during the

This article has been accepted for publication and undergone full peer review but has not been through the copyediting, typesetting, pagination and proofreading process which may lead to differences between this version and the Version of Record. Please cite this article as doi: 10.1029/2018TC004958

Pleistocene is consistent with a change from Nubia-imposed to Adria-imposed convergence indicating that the fragmentation of the Adriatic promontory could have occurred 1-2 Ma ago.

Keywords

Adria microplate; Adriatic promontory; Southern Alps; Shortening-rate; Balanced cross-section; Kinematic change

1. Introduction

The Late Cenozoic evolution of the Mediterranean convergence zone has been mostly driven by the inherited paleogeography of the Tethyan realm, which in turn controlled the first-order segmentation of the plate boundary (Faccenna et al., 2014a). In the E and W, N-dipping subduction of oceanic lithosphere, now preserved in the form of the land locked Ionian Sea basin, resulted in back-arc extension in the Western Mediterranean and Aegean regions starting in the Late Oligocene (Jolivet and Faccenna, 2000) (inset of Figure 1). By contrast, the presence of the Adriatic continental plate N of the Ionian Sea in the Central Mediterranean led to opposite S-dipping subduction of the Eurasian lithosphere below Adria. The ultimate consequence of this segmentation was to decouple the Central Mediterranean from the Western and Eastern Mediterranean by maintaining the locus of plate convergence across the Alps in the former while back-arc extension produced southward migration of the plate boundary in the latters.

Specifically, continental collision continued in the Central Mediterranean through the indentation of the Adriatic promontory (Channell et al., 1979) (inset of Figure 1) while plate convergence in the Western and Eastern Mediterranean was mostly absorbed through the consumption of the Tethyan lithosphere at the trenches. The general outward migration of the trenches in the W and E caused the plate boundary to rotate along the western and eastern sides of the Adriatic promontory (Faccenna et al., 2014a). This caused the promontory to progressively narrow until reaching its present NNW-SSE-elongated shape (inset of the Figure 1). It is therefore important to realize that while the promontory has a prong-like shape at the surface, it is actually more like a large sheet when incorporating the portions of lithosphere that have been subducted to the W beneath the Apennines and to the E beneath the Dinarides.

The Cenozoic motion of the Adriatic promontory is debated. NW-SE trending rifts that opened during the Miocene in the Ionian Sea between Africa and Sicily (Civile et al., 2008, 2010) suggest that the Adriatic promontory could have moved away from Apulia during this time period. Rotation of 5±3° of the Adriatic relative to Eurasia over the last 20 Ma has been inferred from tectonic reconstructions at the scale of the Adriatic promontory (LeBreton et al., 2017) suggesting significant, although little, motion of the promontory relative to Nubia. On the other hand, reconstructed past relative plate positions (e.g Channell et al., 1979; Dewey et al., 1989) and paleomagnetic data (e.g Channell et al., 1996; Rosenbaum et al., 2004) suggest that the narrow band of continental lithosphere, which constitutes the Adriatic promontory, behaved as a rigid prolongation of the Nubia Plate during most of the plate convergence period. Therefore, at the scale of the entire Mediterranean, the northern tip of the Adriatic promontory should represent the most stable converging boundary for the Neogene times, especially when compared to the plate boundary in the E and W. This is supported by the Mediterranean Moho map (see a review of crustal models in Faccenna et al., 2014a),

which clearly shows that the Southern Alps, located at the northern tip of the Adriatic promontory (Figure 1), represent one of the most thickened areas in the entire Mediterranean (the Moho discontinuity is at about 50-km-depth). Therefore, this region of colliding continental plates should represent the place where the total Neogene convergence (all plate and microplate motions are considered in a fixed-Eurasia reference frame in this article) has been best preserved.

Conversely, GPS velocities clearly indicate that the northern part of the Adriatic promontory is now completely detached from Nubia and moves independently from the two major plates in a counterclockwise rotation (e.g Anderson and Jackson, 1987; Calais et al., 2002; D'Agostino et al., 2008; Weber et al., 2010) (inset of the Figure 1). Geodetic data have been used to infer a fragmentation of the promontory into several microplates (Oldow et al., 2002; Sani et al., 2016). In particular, D'Agostino et al. (2008) have suggested that the southern part of the Adriatic promontory could also move independently from the two major plates, possibly defining a second microplate, the Apulian-Ionian-Hyblean (AIH) microplate, rotating clockwise. Along the northern boundary of Adria, the predicted convergence imposed by the rotation of the microplate changes from about 2.5 mm/yr along a NNW-SSE direction in the E to few tenth of mm/yr along a NW-SE direction in the W (e.g D'Agostino et al., 2008; Weber et al., 2010) that is is two to ten times lower than the 5 mm/yr Neogene to present-day Nubia convergence (Calais et al., 2003; Rosenbaum et al., 2002). This means that only a fraction of the present-day plate motion should be absorbed N of the Adriatic promontory.

What is presently controlling the motion of Adria? What initially triggered its own independent motion and when did this occur? D'Agostino et al. (2008) have suggested that the fragmentation of the Adriatic promontory into the Adria microplate has resulted from its narrowing, and consequent weakening, caused by the consumption of the Tethyan lithosphere in the E and W (inset of Figure 1) and speculated a post-Miocene age for this event. Similarly, map-view restoration at the SE boundary of Adria has suggested that coherent motion of the promontory together with Nubia could be resolved for most of the convergence period, with only the last 4 Ma being characterized by the present-day kinematics (Van Hinsbergen and Schmid, 2012). D'Agostino et al. (2008) also showed that the opposite rotations of the Adria and AIH microplates are sufficient to accommodate the Nubia convergence, thus suggesting that the main force controlling the current microplates motion could be the large-scale plates motion. On the other hand, Faccenna and Becker (2010) produced a map of mantle flow generated by density anomalies at the scale of the Mediterranean, which suggests that the motion of Adria could be controlled by the conjugate action of Nubia convergence and eastward pull of the Hellenic slab.

The present study constrains the timing of fragmentation of the Adriatic promontory into the Adria microplate to produce a chronologic background suitable to inform answers to those questions. We focus on the eastern Southern Alps where this fragmentation should have produced a significant decrease in the shortening-rate (Adria-imposed convergence is about half the Nubia-imposed convergence) and thus modified the kinematics of shortening. From a 5-m-DEM, we identify the surface expression of cumulative thrusting and recognize evidence of recent deformation. Such evidence mostly consists of folded alluvial surfaces deposited at the front of the Southern Alps since the Last Glacial Maximum (=LGM). We accurately characterize the geometry of the folds from the 5-m-DEM in the Friuli area (eastern part of the eastern Southern Alps) and infer the structure responsible for those folds at depth. Those

observations allow constructing a balanced geological cross-section suitable to derive post-glacial and average Neogene shortening-rates across the belt. Those results are then compared to the reconstructed plate motion in order to detect when the locus of accommodation of Nubia convergence has moved from N of the Adriatic promontory to more distributed across the convergence zone. This is ultimately used to estimate the age of the fragmentation of the Adriatic promontory.

2. Geologic and morphotectonic setting of the eastern Southern Alps

The eastern Southern Alps consist of an ENE-WSW-oriented mountain belt culminating at 3343 m at the Marmolada. It is limited by the Periadriatic fault in the N, the Northern Dinarides in the ESE and the Veneto-Friuli basin in the S (Figure 1). It represents a back-thrusted wedge of Adriatic crust that developed over the last 14 Ma as a result of indentation of the Adriatic plate (e.g Castellarin et al., 2006; Castellarin and Cantelli, 2000; Doglioni, 1987, Doglioni, 1992; Heberer et al., 2017; Schönborn, 1999) (Figure 2a). The architecture of the eastern Southern Alps shows that the topography grew by stacking of S-vergent thrust faulting, with strike of the fault planes generally bending from NE-SW in the W to NW-SE in the E (Figures 2a, 2b and 2c). The Southern Alps over-thrust the Dinarides, and its associated NW-SE-striking thrusts (e.g. Palmanova thrust of Figure 2a), to the E and the Veneto-Friuli Basin to the S (Figure 2a).

The Veneto-Friuli foreland basin forms a northward thickening clastic wedge (Fontana et al., 2008; Peruzza et al., 2002) that developed during the Miocene in response to syn-tectonic erosion of the growing relief. In the N, rocks of the foreland basin have been uplifted by cumulative thrusting and are locally exposed few tens of meters above the basin, testifying to the southward migration of thrusting over time (Castellarin and Cantelli, 2000; Mellere et al., 2000; Zattin et al., 2006) (Figure 2). Such a general in-sequence migration is also attested by the fact that the amplitude of folding apparently decreases to the S (high tilt of Mesozoic sequences N of the Staro-Selo and Monte Simeone thrusts versus gentler folding of Eocene flysch S of the Staro-Selo thrust, Figure 2c), and the 1976 Friuli seismic sequence (magnitude up to 6.4) likely ruptured the most external Tricesimo thrust (Cheloni et al., 2012) with its epicenter located only 6-7 km from the range-front (Figure 1).

The most recent evolution of the Veneto-Friuli basin consisted of the deposition of fluvio-glacial and fluvial deposits, organized in large coalescing fan-lobes and marking a sharp topographic transition with the relief in the N (Figure 1). Several generations of inset alluvial fans are observed, the timing of deposition and subsequent incision having been largely controlled by the successive advances and retreats of glaciers in the inner parts of the belt during the Late Pleistocene (Fontana et al., 2008). Based on geomorphic observations and ^{14}C-dating, three main phases of fan aggradation have been recognized: Peak LGM (24-18 ka), Late LGM (18-15 ka) and Holocene (post-8 ka) (Fontana et al., 2008), respectively referred to “a2”, “a1” and “a0” in the following sections.

3. Methodology: identifying recent faulting/folding from geomorphic markers

A 5-m-DEM was derived from accurate 1:5000 topographical maps and was used to map alluvial terraces and fans, establish their relative chronology through quantitative morphological analysis (topographic profiles, surface roughness), and assign emplacement ages to them (a0, a1, a2) based on the absolute chronology of Fontana et

al. (2008). DEM analysis also allowed identifying evidence of recent (Late Pleistocene-Holocene) surface deformation, such as tectonic scarps and warped alluvial surfaces, which were in turn used to map the active traces of folds and faults (Figure 1). Most of the mapped active thrusts emerge in the Veneto-Friuli basin and match with structures previously recognized from seismic profiles and structural mapping (e.g Caputo et al., 2010; Peruzza et al., 2002; Poli et al., 2002). The thrust geometry reveals four main active fault segments of 20 to 30 km length (see also Aoudia et al., 2000; Benedetti et al., 2000; Galadini et al., 2005; Monegato and Poli, 2015). Moreover, the analysis failed to detect evidence of recent activation of the internal thrusts (specifically the Staro-Selo and Monte Simeone thrusts, SST and MST in Figure 2) suggesting that shortening is mostly accommodated by slip on faults emerging S of the range-front. In the next sections, we focus on the eastern part of the eastern Southern Alps where we constrain recent deformation associated with the Udine and Tricesimo faults (we also briefly document new observations associated to the Montello fault). This is done by using some of the mapped alluvial surfaces as structural markers, able to accurately record tectonic deformation.

The geomorphology of the studied area largely results from the deposition of moraine ridges of the Tagliamento glacier about 25-20 ka ago, and subsequent outwash deposits (Figure 3). Despite the complex geomorphology of this recessional landscape, two main markers suitable to record Late Pleistocene deformation have been identified. The main preserved fan (a1) of the Torre river is used to constrain deformation associated to the Udine faults (section 4). This fan displays a clear cone shape and is made of gravely to sandy outwash deposits (Fontana et al., 2008). Maps of filtered topography and residual topography of the studied site are provided in the Supporting Information (Figure S1) to show that this surface is characterized by a very planar topography. In particular, there is no evidence of glacial overprints, such as glacially dammed lakes or ice-collapse structures, consistent with the observation that this fan is located S of the most external morainic ridges, is younger than them (Figure 3) and was thus deposited in a time when the Tagliamento glacier had already retreated (Fontana et al., 2008). On the other hand, the alluvial terraces preserved on the sides of the Cormor valley are used to constrain deformation associated to the Tricesimo fault (section 5). Although located within the morainic complex of the Tagliamento glacier, the geometry of this stream and its terraces shows that it clearly represents a post-glacial drainage, with its valley characterized by large meanders and a very constant width (Figure 3).

The aforementioned characteristics of these two geomorphic markers indicate that they have been deposited in a dominantly fluvial environment and were not affected by glacial processes. Hence they could be used as structural makers able to record tectonic deformation, provided that reasonable bounds could be placed on their initial geometry (e.g. Lavé and Avouac, 2000; Meyer et al., 1998).

4. Evidence of active folding in the Veneto-Friuli Basin inferred from post-glacial alluvial fan topography

4.1 The Udine Thrust

S of the Tagliamento moraines, in the eastern part of the study area, the surface of the Veneto-Friuli basin is mostly composed of coalescing a1-fans, deposited by the Torre, Cormor and Nadiza Rivers (Figure 3). This surface is characterized by gentle erosion

localized along rill channels incised by less than 2 m. Patches of more incised (4-8-m-deep gullies) and weathered surfaces (called "a3" in the following) are exposed between Udine and Pozzuolo in the form of two sub-parallel 600-1200-m-wide strings (Buttrio and Pozzuolo zones) trending approximately N295 perpendicular to the drainage (Figure 3). Moreover, those surfaces display steeper slopes on their downstream sides (0.71°) while they appear to merge with a1 upstream. Near Buttrio, on both sides of the Torre river, the a1 surface appears cut by a smooth and continuous escarpment connecting the western and eastern a3-patches of the Buttrio zone and marked by the regressive incision of 3-5-m-deep gullies. Although less prominent, a comparable topographic scarp could be observed across a1 in the prolongation of the Pozzuolo zone and is underlined by similar entrenched gullies channelled at its base.

The Buttrio zone is also in correspondence with the presence of the 2-3-km-long Buttrio hill, which is marked in the SW by a very sharp and rectilinear contact with the alluvial basin (Figures 3a and 3b). The eastern part of the hill is drained by the Buttrio stream which displays a sigmoidal shape (Figure 3c): it flows S, then bends to the SE along the NW-SE-oriented ridge that flanks the SW side of the hill before turning S to exit the relief (Figures 3a and 3c). About 800 m NW of the stream outlet, a NE-SW-oriented wind-gap has been preserved across the ridge (Figure 3c). The observed geometrical relationships suggest that this wind-gap used to drain the Buttrio stream before it acquired its modern course (Figure 3c). The topography of the paleo-channel displays opposite slopes in the SSW and NNE, separated by a section that has been apparently eroded by karstic processes (Figure 3d). The SSW-sloping section of the paleo-channel stands 20 m above the Buttrio stream and is much steeper (2.48° versus 0.45°; Figure 3d) than the active channel suggesting it has been uplifted and tilted to the SW.

From those observations, we infer that the two zones represent the frontal extents of actively rising areas that led to preserve a3-patches above post-glacial surfaces (see Meyer et al. (1998) for an analogous case study in northern Tibet). We therefore interpret the observed topographical scarps as the surface expression of a thrust, the Udine thrust, as previously inferred by Galadini et al. (2005). The accurate geometry of that topographic bulge has been extracted from the 5-m-DEM along 13 parallel a1-profiles oriented parallel to the main topographic gradient (Figure 4a). The resulting swath profile shows that a1 has been folded upstream of each of the two a3-strings. The initial (pre-folding) profile of a1 has been modelled from the two far-field unperturbed sections (Figure 4a) and using the general equation by Morisawa (1968), which describes the longitudinal profiles of rivers as:

$$H = be^{-mL}$$

where b and m are constants, and H represents the decrease in altitude along the river bed (or along the alluvial surface) and L the distance in the downstream direction.

The uplift profile of a1 could then be constructed by computing the difference between observed and modelled initial profiles then projecting it perpendicularly to the fold axis (Figure 4b). The Buttrio anticline is about 12-km-wide and reaches a height of about 5m at the fold hinge (Figure 4b). Moreover it appears asymmetric in cross-section, with an 8.5-km-long 0.03°-sloping back-limb and a 2.5-km-long 0.14°-sloping fore-limb. On the other hand, the Pozzuolo anticline is smaller both in width (about 5.5-km) and height (about 3m) and appears more symmetric, although the geometry is perturbed by rills incision (Figure 4b). Those results show that active folding across the Veneto-Friuli basin has resulted in the uplift of a 17-km-wide 44.8×10^3-m^2-cross-sectional area since

the deposition of the a1 fans (Figure 4b). According to the chronology of Fontana et al. (2008), this amount of folding has thus been accumulated over the last 18-15 ka.

4.2 The Montello thrust

Our fault trace mapping shows that thrust faults emerging in the middle of the basin, similarly to the Udine faults, exist in the western part of the eastern Southern Alps (Figure 1). Benedetti et al. (2000) showed that active thrusting on the NE-SW-striking NW-dipping Montello fault has resulted in folding a flight of Pleistocene terraces preserved at the western edge of the Montello anticline and rerouting the course of the Piave river (Figure 5). The authors also showed that the eastern E-W-oriented section of the Montello anticline has accumulated more shortening than the western NE-SW-oriented section.

The 5-m-DEM shows that the front of the western section is marked by a 10-12-km-long E-W-oriented topographical scarp, which affects Late Pleistocene alluvial fans (Figure 5). We interpret this scarp as the surface expression of the Montello fault, hereafter referred as to the northern Montello fault, which is possibly a blind structure (Benedetti et al., 2000). A 35-km-long linear discontinuous 1-2-m-high scarp, which deforms the regular surface of the Veneto-Friuli Basin, is also identified 8.5 km further in the S between Bassano and Trevise (Figures 1 and 5). This geomorphic feature roughly matches with a tectonic structure mapped from sub-surface data (Caputo et al., 2010) and parallels the northern Montello fault. Therefore, we interpret it as the surface expression of a second fault strand, hereafter referred to as the southern Montello fault.

On the other hand, no similar scarp is observed at the base of the eastern NE-SW-trending section of the Montello anticline (Figure 5). The surface expression of the southern Montello fault is similarly limited to the western part, where the Montello anticline trends E-W (Figure 5). Summing up, there is no detectable evidence of vertical deformation recorded by the recent alluvial fans along the NE-SW-trending section of the Montello anticline.

5. Constraining the geometry of folding above the Tricesimo fault from diachronic geomorphic markers

In the area of Figure 6, where the Tricesimo thrust runs, Quaternary deposits are mainly composed of the moraines of the Tagliamento glacier that flowed from the NW, two pulses of glacial outwash (a1 and a2) fed by the Torre and Cornappo rivers, and late deposits made of narrow surfaces confined on sides of the Cormor channel. According to our mapping and to Zanferrari et al. (2013a), only one pre-LGM terrace is preserved on the left bank of the Torre river (arrow 1 in Figure 6a).

S of Nimis, the distribution of the different alluvial treads shows evidence of recent faulting: while a broad a2 terrace is exposed on the west bank of the Torre river (probably sheltered from river erosion by the moraines relief, 1 km SE of Tricesimo), only a linear 50-100-m-wide string of coeval patches is preserved on the west bank and hangs 10-12-m above the a1 fan (Figure 6). Moreover, this a2-string perfectly underlines the sharp and rectilinear contact that separates the Veneto PreAlps in the NE from the basin in the SW and which has resulted from long-term thrusting above the Tricesimo Thrust (Figure 6) (Zanferrari et al., 2013b). Although the possibility of lateral erosion during a1 deposition could not be definitively ruled out, we interpret the preservation of those surfaces in unsheltered places as the result of cumulative uplift

above the Tricesimo fault. This interpretation is further supported by the presence of a 8-12-m-high SSW-facing scarp (arrow 2 in Figure 6a) observed across a2 on the other side of the river, which roughly aligns with the string of a2-patches. The trace of the 11-km-long segment inferred from those uplifted surfaces ends when reaching the Tagliamento moraines, about 2km NW of Savorgnano. Toward the W, although evidences are mostly subdued across the chaotic relief of the Tagliamento moraines, the trace apparently steps to the SW as revealed by a 5-m-high scarp across a terrace (a1 tread) of the Cormor river (Figure 7a).

Similar to section 4.1, uplift above the Tricesimo thrust has been constrained by the a1 terraces topography of the Cormor river (more details in the caption of Figure 8). From S to N, it reveals two folds placed side-by-side (Figure 8): the 4-km-wide Tricesimo anticline that reaches a height of about 10-m at the fold hinge then gradually drops in the N until merging with the undeformed profile, and the more tenuous incompletely preserved Buia anticline which is 3-4 m high. The scarp associated to the front-limb of the Buia anticline is also observed about 1 km S of Nimis (arrow 3 in Figure 6a). Further in the N, a topographic perturbation across the alluvial terraces of the Torre river could be identified and allows capturing the northern continuation of the Buia anticline. The uppermost and oldest terrace (a3) is preserved 1-2 km S of the Torre canyon outlet on the left bank of the river and stands 35-45m above the present channel (Figures 6 and 7b). The longitudinal topography of that surface exhibits a clear slope-break separating the steep 1.25°-southward-sloping upstream section from the flat to gently northward-sloping downstream stretch (Figures 7b and 8a). To the S, the terrace is degraded by the regressive erosion of a deeply entrenched gully, which abruptly stops at the slope-break (Figure 7a). We interpret those observations as evidence of active uplift and/or northward tilt of the downstream section. The uplift profile of that terrace indicates that its northern and southern sections have been uplifted and tilted to the S and N, respectively (Figure 8b). From this observation we infer that the observed slope-break probably corresponds both to the northern tip of the Buia fold and to the front of a third fold (hereafter referred to as the Bernadia anticline) spreading to the N (Figure 8b).

The absence of preserved terraces along the deep and steeply-sloping Torre and Cornappo canyons, as well as the presence of hanging streams above the Cornappo canyon, strongly suggests this morphology has resulted from high rates of incision, possibly controlled by long-term uplift (Figure 6) (Aoudia et al., 2000). The gorges are carved into a core of Cretaceous limestones, which is topped by a very regular and karstified topographic level composed of 4 distinct surfaces (referred as A, B, C, D in the Figure 7c). Residual topography computed from the 5-m-DEM reveals the distribution and size of the dolines carved in this level (Figure 7c). It shows that the aspect and doline density are very constant from one surface to the other, suggesting that all are parts of a single geomorphic markers.

A NNE-SSW-oriented topographic profile across those landforms has been extracted from the 5-m-DEM. It shows that the surface A is affected by a 20°-slope-break (separating A_1 from A_2 in the Figure 7c) which perfectly reproduces the 20°-tilt of the underlying Cretaceous beds (Zanferrari et al., 2013a) (Figure 8a). Moreover, it clearly appears that the surface B is separated from the surface A by a 70-m-high scarp, itself matching with a 70-m-throw inferred on a NNE-vergent back-thrust by Zanferrari et al. (2013a) (Figure 8a). Finally, surface observations show that both slope-break and topographical scarp have a trend of approximately N320 (Figure 7d).

The match between the topography of the karstic marker and the underlying geological structure suggests either that this marker is a structural surface developed on

carbonate beds of different dips, or that initially it was a flat karstified surface subsequently deformed in the same way as the underlying strata. Because dolines cannot form on local slope steeper than 20° (Williams, 1985) and because dolines density is inversely correlated to the local slope for lower values (Phillips et al., 2003), we find the second explanation much more reasonable. Specifically, we infer that karstification on the 20°-sloping A_1 (where dolines density is similar to A_2, see Figure 7c) had to occur while the local slope was similar to the one of A_2, that is probably nearly horizontal. According to that interpretation, the 20°-tilt is then interpreted as the hinge of the Bernadia anticline, what allows accurately defining the axial surface of that fold (Figure 8a).

Assuming that karst development occurred during the Plio-Pleistocene (Benedetti et al., 2000; Moulin et al., 2016; Mocochain et al., 2009), one can infer that the observed deformation probably took place in the same recent folding pattern than the one inferred from the topography of alluvial terraces. This inference is corroborated by the similarity between the observed N320-trend and the strike of the Tricesimo thrust trace. The 20°-sloping section of the karstic marker would then represent the diachronic northern continuation of the Bernadia anticline front-limb (Figure 8b).

6. Balanced cross-section and Neogene shortening-rates

6.1. Tricesimo thrust geometry and post-glacial shortening-rate

Quantitative morphology analysis showed that the 30-km-wide southern section of the eastern Southern Alps is actively deformed through the growth of five WNW-ESE-oriented anticlines. This folding pattern could then be used to constrain the fault geometry at depth. Three main requirements to satisfy are considered:

- According to Peruzza et al. (2002) folding across the eastern Southern Alps occurred by bed-parallel-slip (fault-bend-folding; Suppe, 1983). Although other styles of folding could exist, the poor resolution of the published seismic profiles (e.g Merlini et al., 2002; Galadini et al., 2005) makes it difficult to estimate how important they are. Therefore the construction of the fault geometry and cross-section assumes that bed-parallel-slip is the only mode of folding at work. The presented interpretation is thus affected by uncertainties, which cannot be quantified with the available data (e.g Bernard et al., 2007).
- From bottom to top (see the right side of Figure 9), the stratigraphic sequence of the eastern Southern Alps is first made of a volcano-sedimentary unit (Upper Permian-Middle Triassic: 3000-3500-m-thick) overlying the crystalline basement and topped by incompetent layers. This unit is unconformably overlain by the Mesozoic carbonatic sequence, which reaches a thickness of about 4500-5000-m and a depth of about 3900m. The sequence ends with the unconformable deposition of the Paleocene-Eocene turbidites, which documents the erosion of the Dinaric orogeny to the WNW. Finally, a Mio-Plio-Pleistocene succession of foreland basin deposits fills the shallowest part of the Veneto Friuli basin. The two unconformities have been recognized as the main decollement horizons (hereafter referred to as D2 (8-9-km-depth) and D1 (4.1-3.7-km-depth)) that have controlled the tectonic structure of the Southern Alps (Peruzza et al., 2002; Schönborn, 1999). The cross-section is hence constructed by assuming that the

main decollement horizons lie along D1 and D2 where drastic changes in the rheological properties occur (Peruzza et al., 2002; Schönborn, 1999) (Figure 9).

- The Palmanova anticline, buried beneath the foreland deposits, is inherited from a former ENE-WSW-directed Oligocene compression and is characterized by an asymmetric shape and a fold hinge located in the vicinity of Pozzuolo (Peruzza et al., 2002) (Figure 9). Therefore, the proposed fault geometry should account for the buckling of the involved rocks.

Udine Thrust Splays

The geometry of the Udine Thrust Splays is assessed by combining the method of mass-conservation, which relates the slip on the fault (S) to the depth of the fault ramp (D) and the uplifted cross-sectional area (A):

$$S = A/D \qquad \text{(equation 1)}$$

with the method of fault-bend-folding (Suppe, 1983), which relates the slip on the fault (S) to the observed uplift (U) and the fault dip (θ):

$$S = U/\sin(\theta) \qquad \text{(equation 2)}$$

For any value of D and provided that a measure of A is available, the combination of equations 1 and 2 allows inferring θ wherever surface uplift has been measured (see Lavé and Avouac (2000) for a detailed comparative description of the two methods):

$$\sin(\theta) = (U*D)/A \qquad \text{(equation 3)}$$

Resolving this equation from the uplift profile of the Figure 5b (providing values for U and A) yields a completely vertical dip when assuming that the Buttrio ramp is rooted into D2, and a more reasonable 35-40°-dip when assuming a decollement along D1. Hence we infer that the growth of the two anticlines is controlled by slip on ramps that emerge from D1, in agreement with the interpretation by Galadini et al. (2005). We further interpret the increasing uplift observed along the back-limb of the Buttrio anticline (Figure 5b) as the expression of a curved geometry of the ramp, itself controlled by the shape of the Palmanova anticline (Figure 9). According to our fault geometry, slip would be sequentially transferred to R1 and R1', controlling the growth of the Buttrio and Pozzuolo anticlines (Figure 9). Note that the geometry of the ramps as shown in Figure 9 is only indicative and could be better constrained with higher resolution seismic profiles. Finally, equation 1 indicates that folding of the a1 surface has resulted from 11.6±1.6 m of slip on D1.

Tricesimo Thrust

Seismic profiles of low resolution (Merlini et al., 2002) suggest the Bernadia anticline is compatible with a fault-bend-fold formed by flattening of a deep ramp (R2) along D1 (called D'1 in the following to distinguish it from the southern D1) (Figure 9), an interpretation that agrees with Aoudia et al. (2000). Projecting the axial surface of that anticline (constrained from the karstic marker, Figure 8) down to D'1 allows determining the top of R2 (lower right inset of the Figure 9). Moreover, this axial surface is directly related to the change in dip from R2 to D'1 (Suppe, 1983). Then the

equations of fault-bend-folding (Suppe, 1983) should apply and allow constraining a dip of about 18° for R2.

The shallowest part of the Tricesimo thrust has been imaged from seismic profiles as a 35-45°N-dipping ramp (R'1 in the Figure 9) (Galadini et al., 2005). While this structure should be responsible for the growth of the Tricesimo anticline (Galadini et al., 2005), the existence of the Buia anticline suggests its geometry changes at depth before connecting to D'1. Specifically, we propose that it is related to slip on a minor intervening flat-ramp geometry (R'1'-D'1') between D1 and R'1 (Figure 9). Knowing the dip of R'1 (40±5°), the dip and length of R'1' are then fully determined (equation 2) by the width of the Buia anticline and by the 0.5-uplift-ratio between the Buia and Tricesimo folds.

Considering the proximity between the Buttrio anticline and the Tricesimo thrust, the three main ramps (R1, R1' and R'1-R'1') are likely to connect via the D'1-D1 decollement. Thus, the amount of post-a1-abandonment slip on D'1 could not be directly quantified from equation 1 because this would require a-priori assumptions on how the slip is partitioned between R'1' and D1. Hence we only used equation 2 and considered a 40±5°-dip for R'1 to estimate the amount of slip able to reproduce the 10-m-uplift of the Tricesimo anticline. It yields 15.7±1.3 m on R'1. Finally, by assuming that slip is conserved from D'1 to R'1' and D1, we found 27.3±2.9 m of slip on D'1 since the abandonment of a1 surfaces.

There is no information available on whether the dip of R2 changes or not at depth. Therefore, we assume a constant 18°-dip down to D2 (Figure 9). Note that this is consistent with the 15-20° dip inferred from triangulation of levelling data associated to the 1976 Friuli earthquake sequence (Cheloni et al., 2012). Downward, it is most probable that the fault flattens when arriving at the incompetent layers of D2 (Peruzza et al., 2002) (Figure 9). The structure of the eastern Southern Alps upper crust has been imaged by the TRANSALP seismic profiles running about 70 km W of our study area (Castellarin et al., 2006) and could be incorporated into our fault geometry. In the deepest parts of the belt, it showed that the upper crust is thrusted along a major 15-20°-dipping ramp (R4 in Figure 9) connected to D2 via an intervening flat-ramp geometry (D3-R3, in Figure 9). Applying the equations depicting the change in slip across fault-bend-folds (Suppe, 1983) indicates that the inferred 27.3±2.9 m of slip on D'1 since the abandonment of a1 alluvial surfaces implies about 25.2±2.7 m of coeval slip on R4. According to the 15.0-18.0-ka-age of the a1 surfaces (Fontana et al., 2008), the shortening-rate at the scale of the belt would thus be 1.5±0.3 mm/yr over the post-LGM period.

The overall fault geometry is compatible with the main features of previously published cross-sections. Only the shallowest geometry of the Tricesimo thrust as pictured in Figure 9 differs from the cross-section presented in Peruzza et al. (2002), Poli et al. (2002) and Galadini et al. (2005). Specifically, this cross-section suggests that each of the anticlines observed N of the Tricesimo thrust (Tricesimo, Buia and Bernadia) are bounded by a N-dipping fault to the S. The fault geometry presented in Figure 9 makes the default choice that these folds are only related to deep bends of the fault plane because i) the available data do not allow deciding if the Buia and Bernadia anticlines are the expression of faults that reach the surface (note that the total slip affected to these faults in the alternative cross-section is insignificant compared to that of the Tricesimo thrust; Peruzza et al., 2002), ii) introducing additional faults would require us to consider a complex out-of-sequence migration of the deformation. We acknowledge that this aspect should be improved in the future. However, it should be noted that this

does not affect the estimation of Late Pleistocene shortening-rate, which is the main purpose of the present article.

6.2. Imbricate thrusts geometry at the scale of the belt and finite shortening

The finite amount of slip on that upper crustal structure has been adjusted to reproduce the shallowest geometry of Figure 2c and the geometry of the Mesozoic/Cenozoic reflector (Merlini et al., 2002) for the Tricesimo thrust, and account for the small displacement of a Lower Miocene reflector (Peruzza et al., 2002; Galadini et al., 2005) for the Udine thrust splays (Figure 9). The rest of the geological section has been drawn by assuming that the two other major thrusts recognized in the area (Monte Simeone and Staro-Selo Thrusts) shared the same geometry than the Tricesimo Thrust, and adjusting the total slip on those two thrusts to reproduce the geological structures observed at the surface (Figure 2) (for example, the Staro-Selo Thrust ramp that emerges at the surface is necessarily the equivalent of R2 and constrains the total shortening (Figure 9)). The assumption of similar thrust geometry is supported by the fact that they cut across the same stratigraphic sequence (Merlini et al., 2002; Peruzza et al., 2002; Poli et al., 2002) and therefore that fault bends should occur along the same horizons (e.g Suppe, 1983). Finally, the amount of slip on the Fella-Sava back-thrust has been adjusted to account for the vertical throw observed at the surface (Carulli, 2006). Note that other minor S-dipping back-thrusts are observed N of the surface trace of the Monte Simeone thrust (Carulli, 2006). Estimating how these back-thrusts connect to the main N-dipping thrusts is not trivial. Hence they were not incorporated into the cross-section. The 43 km of retrieved total shortening (Monte Simeone thrust: 9 km; Staro-Selo thrust: 22 km; Tricesimo thrust: 12 km, 10 km of which being unrelated to slip on the Udine thrust splays) (Figure 9) should thus be considered only as a minimum value. However the amount of slip on these back-thrusts is relatively small (Carulli, 2006) and should add only few kilometres to the inferred value of 43 km.

7. Discussion

7.1. Evolution of shortening kinematics in the eastern Southern Alps from 14 Ma to the present

Our results suggest that NNE-SSW-oriented shortening at a rate of 1.5±0.3 mm/yr since the LGM period has led to folding of alluvial markers of the Veneto-Friuli plain. This value is in agreement with geodetic profiles across the belt (Cheloni et al., 2014; Serpelloni et al., 2016) and suggests that about 75% of Adria-imposed convergence is absorbed across the eastern Southern Alps. While it appears that slip is equally shared between the main Tricesimo thrust (15.7±1.3 m) and the Udine thrust splays (11.6±1.6 m) over the last 15-18-ka, the balanced cross-section shows that the total slip transferred to the Udine thrust splay is very low compared to the entire structure (900-1200 m versus about 12 km; see Figure 9) suggesting the Udine thrust splay has been recently activated. Assuming a constant slip-rate, the age of inception would be about 1-2 Ma.

On the other hand, our balanced cross-section implies a total N-S-shortening of about 43 km. Considering that additional back-thrusting has been neglected in constructing our cross-section, this should be considered as a minimum value, in agreement with the 46-

km-value recorded in the western Southern Alps by Schmid et al., (1996). Based on syn-tectonic sedimentation (Castellarin et al., 1992) and thermochronologic data (Heberer et al., 2017; Zattin et al., 2006), the preferred estimate for the onset of thrusting in the Southern Alps is about 14 Ma, thus yielding a long-term shortening-rate of about 3 mm/yr, two times higher than the post-glacial shortening-rate. If, assuming on the other hand, that thrusting initiated as early as 21 Ma at the onset of Adria indentation (Pomella et al., 2012), then the long-term mean shortening-rate would be of 2 mm/yr, which is still higher than the post-glacial rate. Extrapolating this value back in time and assuming in-sequence propagation of thrusting (Castellarin and Cantelli, 2000; Mellere et al., 2000; Zattin et al., 2006) indicates that slip on the Monte Simeone thrust would have stopped at 11 Ma along with activation of the Staro-Selo thrust (age of slip inception on the Staro-Selo thrust would become 16.5 Ma if considering the upper bound of 21 Ma for the onset of thrusting in the Southern Alps). It is noteworthy that slip on the Monte Simeone stopped after only 9 km of displacement, while the Staro-Selo thrust, of similar inferred geometry, accommodated a finite displacement as large as 22 km (Figure 9). This suggests that activity of the Monte Simeone thrust stopped as a result of external forces rather than of internal dynamics of the growing wedge. We speculate that this external force could have been the last major change in the Nubia/Eurasia convergence, which occurred at 11 Ma (Reilinger and McClusky, 2011) in agreement with our preferred estimate for the onset of slip on the Staro-Selo thrust. Onset of slip on the Tricesimo thrust is thought to have occurred in the Messinian (7-5 Ma) (Castellarin and Cantelli, 2000). Again assuming purely in-sequence migration of thrusting, the 22 km of displacement on the Staro-Selo thrust would have accumulated between 16.5-11 and 7-5 Ma, yielding a shortening-rate of 3.7±1.8 mm/yr. On the other hand, from the 12 km of displacement inferred for the Tricesimo thrust, only 10 km have been accommodated before the activation of the Udine thrust splays that is before our estimate of 1-2 Ma. Assuming that these 10 km of displacement have accumulated between 7-5 and 1-2 Ma, a shortening-rate of 2.5±0.8 mm/yr is inferred. Summing up, shortening accommodated by thrusting in the Southern Alps is constrained to range between 2 and 4 mm/yr over various time-scales except for the most recent period (post-LGM and probably post-1-2 Ma) where it is only 1.5 mm/yr in agreement with geodetic data.

At the scale of the entire eastern Southern Alps, the geometry of thrusting appears constant from one thrust to the other. Specifically, there is a bend in the thrusts geometry from E-W- (in the E) to NE-SW-orientation (in the W) well seen about 15 km W of Tolmezzo (Figure 2). This change in orientation correlates with the western tip of the Fella-Sava back-thrust (Figure 2) for which a right-lateral component of about 1 mm/yr has been inferred from geodetic data (Serpelloni et al., 2016). We thus interpret the bent geometry of the thrusts as suggesting that the long-term deformation across the eastern part of the eastern Southern Alps has been partitioned between SSW-thrusting and E-W-oriented right-lateral motion, allowing accommodation of a general NW-SE-convergence at the scale of the entire belt (Castellarin and Cantelli, 2000; Schönborn, 1999), in agreement with micro-tectonic analyses (Caputo et al., 2010).

Only one structure, the Montello thrust, appears to deviate from this bent pattern of thrusts. Similar to the Udine thrust splays, they emerge 15-20 km away from the range-front and deform the basin surface along two branches (Figures 1 and 5). The northern one, studied in detail by Benedetti et al. (2000), is expressed as the Montello anticline bending from a NE-SW-orientation in the E to an E-W-orientation in the W with cumulative uplift increasing westward, suggesting that the E-W section has

accommodated more shortening than the NE-SW section (Benedetti et al., 2000). The southern frontal branch parallels the E-W-trending section of the northern branch, then vanishes in the E (Figure 5 and section 4). From those observations, we speculate that the two branches are the surface expression of two propagating thrust splays emerging from a single main thrust at depth, probably rooted at about 12-13-km-depth (Castellarin et al., 2006; Galadini et al., 2005; Priolo et al., 2015).

Moreover, no surface faulting can be detected NNE of Trevise along the southern branch (Figures 1 and 5) (that one could expect to parallel the NE-SW-striking section of the northern branch) suggesting again a lower uplift above the NE-SW-striking section of the thrust. This is further confirmed by geodetic data, which show that a lower rate of shortening as well as a 1 mm/yr left-lateral component is accommodated across the NE-SW-oriented section (Maniago segment and northeastern part of the Montello segment) of the frontal thrust zone (Serpelloni et al., 2016). Moreover, left-lateral motion along this section of the belt agrees with the distribution of fault-plane solutions during the 3 years that followed the 1976 main shock of the Friuli sequence: specifically, sinistral focal mechanisms (M_L from 3.4 to 4.5) were found to align in a NE-SW trend parallel to the NE-SW section of the Piave river (Slejko et al., 1999). Kinematically, this implies that the direction of Late Pleistocene to present shortening is N-S oriented, contrasting with the long-term NW-SE-compression inferred from the large-scale structure of the belt.

Inception of slip on the Montello thrust is thought to have occurred in the Pleistocene (Benedetti et al., 2000; Caputo et al., 2010), similar to the Udine Thrust splays. Such a young activation could be consistently related to the fact that the Maniago thrust has the strongest large-scale geomorphic expression (Figure 1) despite the significantly lower shortening-rate it absorbs (Serpelloni et al., 2016). On the other hand, micro-tectonic analyses documented a shift in the direction of maximum compression from N314 during the Pliocene to N340 during the Pleistocene (Caputo et al., 2010). Together, those observations suggest that the long-term NW-SE-convergence (e.g Caputo et al., 2010; Castellarin and Cantelli, 2000) has recently (1-2Ma) changed to a N-S-convergence and been marked by the activation of the Montello thrust. The contemporaneity of inception of slip along the Udine thrust splays suggests a similar origin.

We propose that new deeply rooted thrusts (Montello thrust at 12-13 km depth) were activated in the W because of the unfavourable NW-SE-orientation of the older structures (Figure 2), while in the E the change in the direction of compression could have been simply compensated by a decrease in the right-lateral component along the Fella-Sava Back-thrust (Figure 1), therefore not requiring the growth of a new deeply rooted thrust. We speculate that the activation of the Udine Thrust Splays, shallowly connected to the Tricesimo Thrust, occurred only to maintain some lateral continuity of the frontal thrust zone (Figure 1).

Caputo et al. (2010) showed that to first order the direction of compression in the eastern Southern Alps co-varied with the trajectory of Nubia with respect to Eurasia over the last 10 Ma, suggesting that plate convergence has been the main driver of shortening kinematics during this period. This is in agreement with the inference that thrusting on the Monte Simeone thrust probably stopped at about 11 Ma, the period of the last important change in the Nubia/Eurasia convergence (Reilinger and McClusky, 2011 and references therein). More specifically, the direction of compression has been affected by two events of clockwise rotation, one in the Messinian and one in the Pleistocene (Caputo et al., 2010). The first one appears to be coeval with a clockwise rotation of the direction of plate convergence while the second one is coeval with a

slight counter-clockwise rotation of the direction of convergence (Caputo et al., 2010; their Figure 12). Summing up, this counter-clockwise rotation of the direction of plate convergence is the only known Pleistocene change in the Nubia/Eurasia rotation pole (Calais et al., 2003), is marked by a change in the direction of convergence opposite to that we observe and does not significantly change its rate (Figure 10a). Therefore we infer that the transfer of Nubia convergence to the N became more complex about 1-2Ma ago. Caputo et al. (2010) argued for an effect of the Apennines accretionary wedge to account for the Pleistocene change in shortening kinematics. Pointing out that the observed change matches very well with a shift from Nubia-imposed to Adria-imposed convergence (blue and red vectors in Figure 10a), we suggest an alternative explanation, in which this change is simply a result of the fragmentation of the Adriatic promontory into the Adria microplate.

7.2. Crustal shortening and plate motion over the Neogene

We now attempt to estimate the age of the Adria microplate by comparing the Neogene plate convergence (Nubia with respect to Eurasia) with the total coeval amount of shortening absorbed between the Adriatic promontory (Nubia) and stable Eurasia. We choose the Neogene because total shortening across this part of the Alps is best documented for this specific period, and because it represents a time window, which clearly corresponds to post-collisional deformation. This analysis is interested in comparing finite predicted and observed convergence at the scale of an entire section of the Alps and is thus neither affected by temporal fluctuations in the rate of displacement on specific faults or fault systems nor in fluctuations in the rate of plate convergence, which could have occurred during the analysed time window. In line with the foregoing, this analysis is only valid if the Adriatic promontory behaved as a rigid prolongation of Nubia at least from the Early Miocene and until it was fragmented into the microplates configuration, which is presently observed from geodetic data. On the contrary, any event of significant divergence between the Adriatic promontory and Nubia would lead to a surplus of convergence (relative to the convergence of Nubia) at the northern tip of the promontory, and hence the following analysis would result in an underestimation of the age of the fragmentation.

The total shortening assessed across the eastern Southern Alps is at least 43 km (42 km in a N-S-direction). Even if considering the upper bound for the age of thrusting inception (see previous section), this deformation clearly post-dates the Oligocene and more probably represents the accommodation of Adria convergence over the last 14Ma. The remaining Neogene convergence has been essentially absorbed by eastward extrusion of the Eastern Alps (e.g Frisch et al., 1998; Linzer et al., 2002; Ratschbacher et al., 1991). Crustal deformation in this sector of the Alps is probably older than that in the Southern Alps (Heberer et al., 2017) and accounts for 61-64 km of N-S-shortening (Linzer et al., 2002). The last source of Neogene shortening is represented by thrusting in the Northern Alps and accounts for about 10 km of N-S-shortening (Linzer et al., 2002 and references therein) (Figure 10c). Summing these estimates yields a minimum of 113-116 km of N-S shortening absorbed between the Adriatic and Eurasian lithospheres over the Neogene, this period encompassing both the times when Adria was still a Nubian promontory and when it moved as an independent microplate (Figure 10b).

By comparison, the coeval N-S-component of the Nubia/Eurasia convergence, calculated from rotation parameters of Rosenbaum et al. (2002) at the latitude/longitude of the

studied area, is 125 km (mean convergence rate of about 5 mm/yr) and represents the total value that should be retrieved from observed shortening if the Nubia motion was rigidly transferred through Adria throughout the considered time-period (Figure 10). We know that this latter assumption is not valid since the current N-S-component of convergence of Adria is 2-3mm/yr (that is 2-3km/Ma) lower than the N-S-component of convergence of Nubia (Figure 10a). Hence the 9-12-km-maximum deficit of shortening (125 km - 116 km or 125 km - 113 km) yields an equivalent time-period of 3-6Ma, which could be interpreted as a timing estimate for the onset of the Adria rotation, keeping in mind that this is a maximum age. Considering the uncertainties associated to all measurements this timing is only indicative, but it strongly suggests that the fragmentation of the Adriatic promontory has occurred very recently, in agreement with D'Agostino et al. (2008). It is also very consistent with the 4 Ma inferred for the onset of the present-day configuration by van Hinsbergen and Schmid (2012).

On the other hand, the consistency of ages (1-2Ma versus a maximum of 3-6Ma) obtained from two independent methods supports the assumption that the activation of new thrusts in the eastern Southern Alps and associated kinematic change about 1-2Ma ago without direct correlation with a change in the Nubia/Eurasia motion, has resulted from the fragmentation of the Adriatic promontory into the Adria microplate. In line with this scenario, we propose that the shift from 2-4 mm/yr (as calculated from the cross-section) to 1.5 mm/yr of shortening (inferred from post-glacial folding) has occurred at the same time as a consequence of the slower motion of the microplate. This is also supported by the fact that many of the Apennines normal faults that presently accommodate the rotation of Adria along its western boundary have been activated roughly at the same time (Galadini, 1999), and that an increase in the strike-slip component of motion along the northeastern boundary of the Adriatic promontory is observed at about 1Ma (Moulin et al., 2016), and could correspond to a dramatic reorganization of tectonic blocks motion related to the onset of Adria rotation at that time.

Although this is beyond the scope of the present article, it should be noted that the good consistency between predicted convergence and observed coeval shortening N of the Adriatic promontory indicates that the amount of distributed deformation within the Adriatic lithosphere is rather small, except if assuming that Neogene divergence between the Adriatic promontory and the Nubia plate is large (independent motion of the promontory). This in turn suggests that the zone of deformation observed in the Central Adriatic, and interpreted as the possible boundary between the Adria and Apulian-Ionian-Hyblean microplates (D'Agostino et al., 2008), is either characterized by very low strain rates or has been activated very recently. The latter inference would be consistent with the scenario proposed above.

To our knowledge, the only study that has carefully discussed the origin of the fragmentation of the Adriatic promontory is the one by D'Agostino et al. (2008). It suggested that its progressive narrowing, caused by consumption of the lithosphere beneath the Apennines, has resulted in reaching a critical width unable to support rigid transfer of Nubia convergence toward the N. If correct, our inference that the inception of Adria rotation occurred about 1-2 Ma ago indicates that it is roughly coeval with slab detachment and slab tear propagation beneath the Apennines (Faccenna et al., 2014b). This suggests that the two processes could be genetically linked, raising new questions related to the interplay between deep mantle and crustal processes.

Conclusion

The traces of the active thrusts in the eastern Southern Alps and the geometry of associated folding have been mapped and characterized from a 5-m-DEM. When combined with geological and geophysical data, the folding pattern recorded by post-LGM alluvial surfaces in the eastern part of the belt allows interpreting that the thrust geometry at depth is made of a main branch emerging at the front of the relief and a shallower thrust splay propagating southward. We extrapolated this geometry to the older internal thrusts to balance a crustal-scale cross-section. Interpretations of that section indicate a shortening-rate of about 1.5mm/yr over the last 18-15 ka and suggest a recent activation of the frontal thrust splays at 1-2Ma, the associated kinematic change being consistent with a shift from Nubia-imposed to Adria-imposed shortening. The minimum 43 km of N-S-shortening yielded by the geological cross-section suggests that shortening absorbed N of the Adriatic promontory is indiscernible from the coeval amount of Nubia convergence and hence that the low convergence presently imposed by the rotation of Adria is a very young process. From those inferences, we ultimately suggest that the kinematic change observed at 1-2 Ma reflects the fragmentation of the Adriatic promontory into the Adria microplate.

Acknowledgements

Our work was partly funded by the INSU-CNRS (project entitled SLORISK resp. L. Benedetti) and by OT Med FEARS project. The Friuli-Venezia Giulia region is acknowledged for providing open-access vectorized 1:5000 topographical maps. We acknowledge Laura Peruzza, Maria Eliana Poli, Fabrizio Galadini, Adriano Zanferrari and Carlo Doglioni for sharing their understanding of the Southern Alps tectonics. We are also grateful to Alessandro Fontana, who took the time to provide detailed answers on the chronology of alluvial fans in the studied area. We greatly appreciated the advice of Jean-Philippe Avouac in balancing the geological cross-section. Vectorized topographic maps used to construct the DEM presented in this study could be accessed at http://irdat.regione.fvg.it/WebGIS/GISViewer.jsp. Readers are welcome to contact the corresponding author (adridri777@gmail.com) for any inquiry regarding the present study.

References

Anderson, H., & Jackson, J. (1987). Active tectonics of the Adriatic region. *Geophysical Journal International*, *91*(3), 937-983.

Aoudia, A., Saraò, A., Bukchin, B., & Suhadolc, P. (2000). The 1976 Friuli (NE Italy) thrust faulting earthquake: a reappraisal 23 years later. *Geophysical Research Letters*, *27*(4), 573-576.

Benedetti, L., Tapponnier, P., King, G. C., Meyer, B., & Manighetti, I. (2000). Growth folding and active thrusting in the Montello region, Veneto, northern Italy. *Journal of Geophysical Research: Solid Earth (1978–2012)*, *105*(B1), 739-766.

Bernard, S., Avouac, J.-P., Dominguez, S., Simoes, M. (2007). Kinematics of fault-related folding from sandbox experiments. *Journal of Geophysical Research : Solid Earth,* 112, B03S12.

Calais, E., Nocquet, J. M., Jouanne, F., & Tardy, M. (2002). Current strain regime in the Western Alps from continuous Global Positioning System measurements, 1996–2001. *Geology*, *30*(7), 651-654.

Calais, E., DeMets, C., & Nocquet, J. M. (2003). Evidence for a post-3.16-Ma change in Nubia–Eurasia–North America plate motions?. *Earth and Planetary Science Letters*, *216*(1), 81-92.

Caputo, R., Poli, M. E., & Zanferrari, A. (2010). Neogene–Quaternary tectonic stratigraphy of the eastern Southern Alps, NE Italy. *Journal of Structural Geology*, *32*(7), 1009-1027.

Carulli, G. B. (2006). Carta geologica del Friuli Venezia Giulia. *Scala*, *1*, 150000.

Castellarin, A., & Cantelli, L. (2000). Neo-Alpine evolution of the southern Eastern Alps. *Journal of Geodynamics*, *30*(1), 251-274.

Castellarin, A., Nicolich, R., Fantoni, R., Cantelli, L., Sella, M., & Selli, L. (2006). Structure of the lithosphere beneath the Eastern Alps (southern sector of the TRANSALP transect). *Tectonophysics*, *414*(1), 259-282.

Channell, J. E. T., d'Argenio, B., & Horvath, F. (1979). Adria, the African promontory, in Mesozoic Mediterranean palaeogeography. *Earth-Science Reviews*, *15*(3), 213-292.

Channell, J. E. T. (1996). Palaeomagnetism and palaeogeography of Adria. *Geological Society, London, Special Publications*, *105*(1), 119-132.

Cheloni, D., D'Agostino, N., & Selvaggi, G. (2014). Interseismic coupling, seismic potential, and earthquake recurrence on the southern front of the Eastern Alps (NE Italy). *Journal of Geophysical Research: Solid Earth*, *119*(5), 4448-4468.

Cheloni, D., D'Agostino, N., D'Anastasio, E., & Selvaggi, G. (2012). Reassessment of the source of the 1976 Friuli, NE Italy, earthquake sequence from the joint inversion of high-precision levelling and triangulation data. *Geophys. J. Int.*, *190*, 1279–1294.

Civile, D., Lodolo, E., Tortorici, L., Lanzafame, G., & Brancolini, G. (2008). Relationships between magmatism and tectonics in a continental rift: the Pantelleria Island region (Sicily Channel, Italy). *Marine Geology*, *251*(1-2), 32-46.

Civile, D., Lodolo, E., Accettella, D., Geletti, R., Ben-Avraham, Z., Deponte, M., ... & Romeo, R.

(2010). The Pantelleria graben (Sicily Channel, Central Mediterranean): an example of intraplate 'passive'rift. *Tectonophysics*, *490*(3-4), 173-183.

D'agostino, N., Avallone, A., Cheloni, D., D'anastasio, E., Mantenuto, S., & Selvaggi, G. (2008). Active tectonics of the Adriatic region from GPS and earthquake slip vectors. *Journal of Geophysical Research: Solid Earth (1978–2012)*, *113*(B12).

Dewey, J. F., Helman, M. L., Knott, S. D., Turco, E., & Hutton, D. H. W. (1989). Kinematics of the western Mediterranean. *Geological Society, London, Special Publications*, *45*(1), 265-283.

Doglioni, C., & Bosellini, A. (1987). Eoalpine and mesoalpine tectonics in the Southern Alps. *Geologische Rundschau*, *76*(3), 735-754.

Doglioni, C. (1992). The Venetian Alps thrust belt. In *Thrust tectonics* (pp. 319-324). Springer Netherlands.

Faccenna, C., & Becker, T. W. (2010). Shaping mobile belts by small-scale convection. *Nature*, *465*(7298), 602-605.

Faccenna, C., Becker, T. W., Auer, L., Billi, A., Boschi, L., Brun, J. P., ... & Piromallo, C. (2014a). Mantle dynamics in the Mediterranean. *Reviews of Geophysics*, *52*(3), 283-332.

Faccenna, C., Becker, T. W., Miller, M. S., Serpelloni, E., & Willett, S. D. (2014b). Isostasy, dynamic topography, and the elevation of the Apennines of Italy. *Earth and Planetary Science Letters*, *407*, 163-174.

Fontana, A., Mozzi, P., & Bondesan, A. (2008). Alluvial megafans in the Veneto-Friuli Plain: evidence of aggrading and erosive phases during Late Pleistocene and Holocene. *Quaternary International*, *189*(7).

Frisch, W., Kuhlemann, J., Dunkl, I., & Brügel, A. (1998). Palinspastic reconstruction and topographic evolution of the Eastern Alps during late Tertiary tectonic extrusion. *Tectonophysics*, *297*(1), 1-15.

Galadini, F. (1999). Pleistocene changes in the central Apennine fault kinematics: a key to decipher active tectonics in central Italy. *Tectonics*, *18*(5), 877-894.

Galadini, F., Poli, M. E., & Zanferrari, A. (2005). Seismogenic sources potentially responsible for earthquakes with M≥ 6 in the eastern Southern Alps (Thiene-Udine sector, NE Italy). *Geophysical Journal International*, *161*(3), 739-762.

Heberer, B., Reverman, R. L., Fellin, M. G., Neubauer, F., Dunkl, I., Zattin, M., ... & Brack, P. (2017). Postcollisional cooling history of the Eastern and Southern Alps and its linkage to Adria indentation. *International Journal of Earth Sciences*, *106*(5), 1557-1580.

Jolivet, L., & Faccenna, C. (2000). Mediterranean extension and the Africa-Eurasia collision. *Tectonics*, *19*(6), 1095-1106.

Lavé, J., & Avouac, J. P. (2000). Active folding of fluvial terraces across the Siwaliks Hills, Himalayas of central Nepal. *Journal of Geophysical Research: Solid Earth (1978–2012)*, *105*(B3), 5735-5770.

Le Breton, E., Handy, M. R., Molli, G., & Ustaszewski, K. (2017). Post-20 Ma Motion of the Adriatic Plate: New Constraints From Surrounding Orogens and Implications for Crust-Mantle Decoupling. *Tectonics*.

Linzer, H. G., Decker, K., Peresson, H., Dell'Mour, R., & Frisch, W. (2002). Balancing lateral orogenic float of the Eastern Alps. *Tectonophysics*, *354*(3), 211-237.

Mellere, D., Stefani, C., & Angevine, C. (2000). Polyphase tectonics through subsidence analysis: the Oligo-Miocene Venetian and Friuli Basin, north-east Italy. *Basin research*, *12*(2), 159-182.

Merlini, S., Doglioni, C., Fantoni, R., & Ponton, M. (2002). Analisi strutturale lungo un profilo geologico tra la linea Fella-Sava e l'avampaese adriatico (Friuli Venezia Giulia-Italia). *Mem. Soc. Geol. It*, *57*, 293-300.

Meyer, B., Tapponnier, P., Bourjot, L., Metivier, F., Gaudemer, Y., Peltzer, G., … & Zhitai, C. (1998). Crustal thickening in Gansu-Qinghai, lithospheric mantle subduction, and oblique, strike-slip controlled growth of the Tibet plateau. *Geophysical Journal International*, 135(1), 1-47.

Mocochain, L., Audra, P., Clauzon, G., Bellier, O., Bigot, J. Y., Parize, O., & Monteil, P. (2009). The effect of river dynamics induced by the Messinian Salinity Crisis on karst landscape and caves: example of the Lower Ardeche river (mid Rhone valley). *Geomorphology*, *106*(1), 46-61.

Monegato, G., Ravazzi, C., Donegana, M., Pini, R., Calderoni, G., & Wick, L. (2007). Evidence of a two-fold glacial advance during the last glacial maximum in the Tagliamento end moraine system (eastern Alps). *Quaternary Research*, *68*(2), 284-302.

Monegato, G., & Poli, M. E. (2015). Tectonic and climatic inferences from the terrace staircase in the Meduna valley, eastern Southern Alps, NE Italy. *Quaternary Research*, *83*(1), 229-242.

Morisawa, M. (1968). Streams; their dynamics and morphology.

Moulin, A., Benedetti, L., Rizza, M., Jamsek Rupnik, P., Gosar, A., Bourlès, D., … & Ritz, J.F. (2016). The Dinaric fault system : Large-scale structure, rates of slip and Plio-Pleistocene evolution of the transpressive northeastern boundary of the Adria microplate. *Tectonics*, 35(10), 2258-2292.

Oldow, J. S., Ferranti, L., Lewis, D. S., Campbell, J. K., d'Argenio, B., Catalano, R., ... & Aiken, C. L. V. (2002). Active fragmentation of Adria, the north African promontory, central Mediterranean orogen. *Geology*, *30*(9), 779-782.

Peruzza, L., Poli, M. E., Rebez, A., Renner, G., Rogledi, S., Slejko, D., & Zanferrari, A. (2002). The 1976–1977 seismic sequence in Friuli: new seismotectonic aspects. *Mem. Soc. Geol. It*, *57*, 391-400.

Phillips, J. D., Martin, L. L., Nordberg, V. G., & Andrews, W. A. (2004). Divergent evolution in fluviokarst landscapes of central Kentucky. *Earth Surface Processes and Landforms*, *29*(7), 799-819.

Poli, M. E., Peruzza, L., Rebez, A., Renner, G., Slejko, D., & Zanferrari, A. (2002). New seismotectonic evidence from the analysis of the 1976-1977 and 1977-1999 seismicity in Friuli (NE Italy). *Boll. Geof. Teor. Appl*, *43*(1-2), 53-78.

Pomella, H., Stipp, M., & Fügenschuh, B. (2012). Thermochronological record of thrusting and strike-slip faulting along the Giudicarie fault system (Alps, Northern Italy). *Tectonophysics*, *579*, 118-130.

Priolo, E., Romanelli, M., Linares, M. P., Garbin, M., Peruzza, L., Romano, M. A., ... & Fabris, P. (2015). Seismic monitoring of an underground natural gas storage facility: The Collalto Seismic Network. *Seismological Research Letters*, *86*(1), 109-123.

Ratschbacher, L., Frisch, W., Linzer, H. G., & Merle, O. (1991). Lateral extrusion in the Eastern Alps, part 2: structural analysis. *Tectonics*, *10*(2), 257-271.

Reilinger, R., & McClusky, S. (2011). Nubia–Arabia–Eurasia plate motions and the dynamics of Mediterranean and Middle East tectonics. *Geophysical Journal International*, *186*(3), 971-979.

Rosenbaum, G., Lister, G. S., & Duboz, C. (2002). Relative motions of Africa, Iberia and Europe during Alpine orogeny. *Tectonophysics*, *359*(1), 117-129.

Rosenbaum, G., Lister, G. S., & Duboz, C. (2004). The Mesozoic and Cenozoic motion of Adria (central Mediterranean): a review of constraints and limitations. *Geodinamica Acta*, *17*(2), 125-139.

Sani, F., Vannucci, G., Boccaletti, M., Bonini, M., Corti, G., & Serpelloni, E. (2016). Insights into the fragmentation of the Adria Plate. *Journal of Geodynamics*, *102*, 121-138.

Schmid, S. M., Pfiffner, O. A., Froitzheim, N., Schönborn, G., & Kissling, E. (1996). Geophysical-geological transect and tectonic evolution of the Swiss-Italian Alps. *Tectonics*, *15*(5), 1036-1064.

Schönborn, G. (1999). Balancing cross sections with kinematic constraints: the Dolomites (northern Italy). *Tectonics*, *18*(3), 527-545.

Serpelloni, E., Vannucci, G., Anderlini, L., & Bennett, R. A. (2016). Kinematics, seismotectonics and seismic potential of the eastern sector of the European Alps from GPS and seismic deformation data. *Tectonophysics, 688*, 157-181.

Suppe, J. (1983). Geometry and kinematics of fault-bend folding. *American Journal of science*, *283*(7), 684-721.

Hinsbergen, D. J., & Schmid, S. M. (2012). Map view restoration of Aegean–West Anatolian accretion and extension since the Eocene. *Tectonics*, *31*(5).

Weber, J., Vrabec, M., Pavlovčič-Prešeren, P., Dixon, T., Jiang, Y., & Stopar, B. (2010). GPS-derived motion of the Adriatic microplate from Istria Peninsula and Po Plain sites, and geodynamic implications. *Tectonophysics*, *483*(3), 214-222.

Williams, P. W. (1985). Subcutaneous hydrology and the development of doline and cockpit karst. *Zeitschrift fur Geomorphologie*, *29*(4), 463-482.

Zanferrari, A., Masetti, D., Monegato, G., & Poli, M. E. (2013a). Note illustrative della Carta Geologica d'Italia alla scala 1: 50.000; Foglio 049 "Gemona del Friuli". *ISPRA-Servizio Geologico d'Italia-Regione Autonoma Friuli-Venezia Giulia*.

Zanferrari, A., Avigliano, R., Monegato, G., Paiero, G., & Poli, M.E. (2013b). Note illustrative della Carta Geologica d'Italia alla scala 1: 50.000; Foglio 066 "Udine". *ISPRA-Servizio Geologico d'Italia-Regione Autonoma Friuli-Venezia Giulia*.

Zattin, M., Cuman, A., Fantoni, R., Martin, S., Scotti, P., & Stefani, C. (2006). From Middle Jurassic heating to Neogene cooling: The thermochronological evolution of the southern Alps. *Tectonophysics*, *414*(1-4), 191-202.

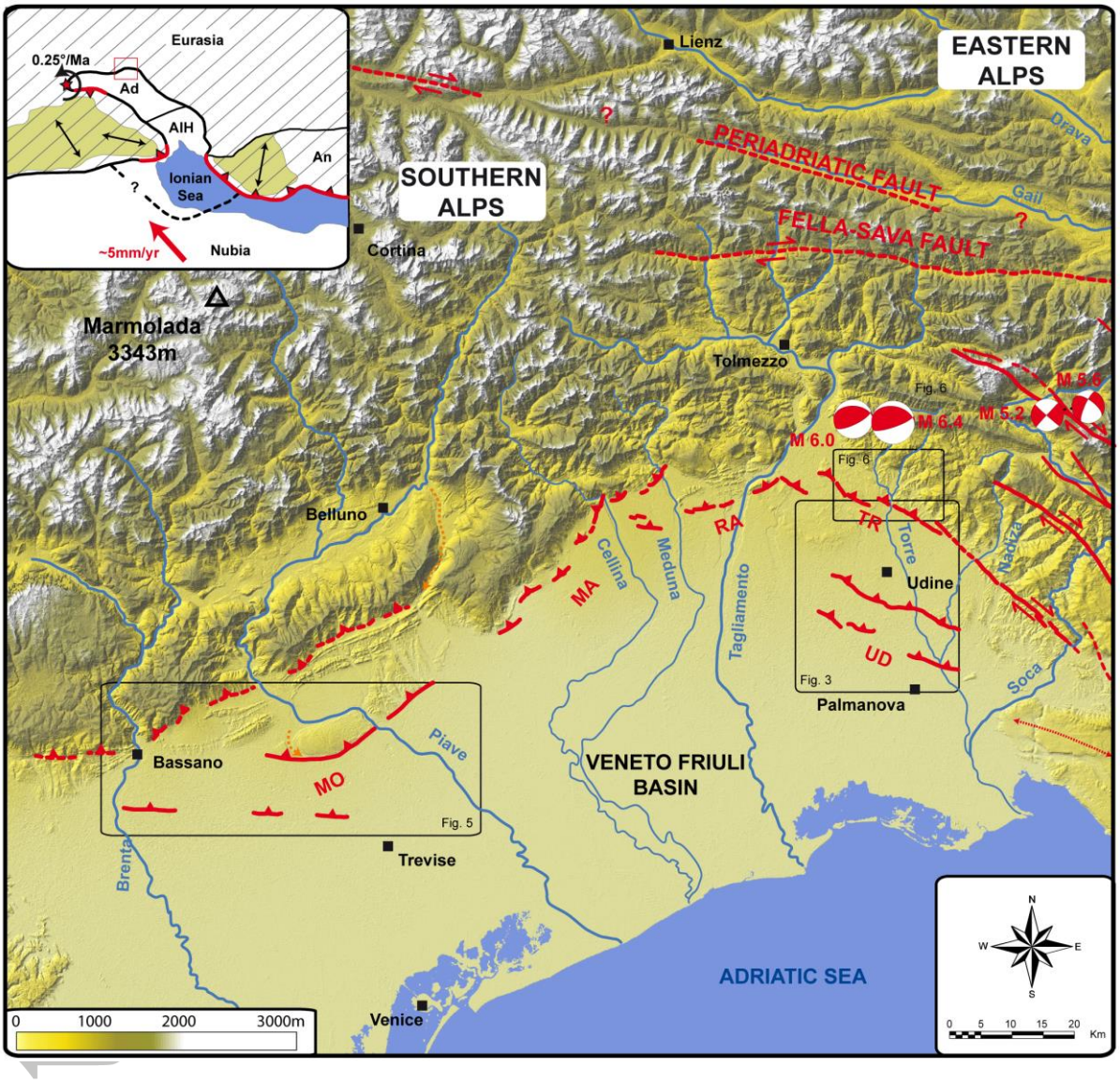

Figure 1: Seismotectonic map of the ESA. Thick black lines represent the active faults (right-lateral strike-slip faults in the eastern part are from Moulin et al. (2016), the Montello Thrust from Benedetti et al. (2000)). The thick dashed line in the vicinity of Bassano refers to the Bassano Thrust for which we no evidence of recent deformation has been identified. Other thrusts are from the present study and have been mapped from 5-m-DEM. Four main segments are identified from this mapping: from E to W they are the 22-km-long ESE-WNW-oriented Tricesimo segment made of three sub-parallel fault branches, the 24-km-long WSW-ENE-oriented Ragogna segment, the 35-km-long NNE-SSW-oriented Maniago segment and the 32-km-long WSW-ENE-oriented Montello segment made of two sub-parallel fault branches. The dashed orange arrow E of Bassano shows the paleo-course of the Piave (Benedetti et al., 2000) and the orange arrow E of Belluno shows another probable paleo-course of the Piave. Thrust segments are labelled as follows: TR=Tricesimo, UD-Udine, RA=Ragogna, MA=Maniago, MO=Montello. Inset shows the simplified geodynamics of the Central Mediterranean: the remnant of Tethyan lithosphere (Ionian Sea) is shown in blue. Thick black and red lines respectively show the former and active subduction zones, representing the long-term plate boundary between Eurasia

(hatched area) and Nubia. Thin black lines represent the Adria (Ad) and Anatolia (An) microplates boundaries. Dotted black line represent the possible boundary of the Apulian-Ionian-Hyblean (AIH) microplate according to D'agostino et al. (2008). The Ad and AIH microplates together define the Adriatic promontory. The yellow areas with double arrows show zones of post-Oligocene extension. The star shows the mean location of the Adria rotation pole with respect to stable Europe. The red box shows the location of the main Figure 1.

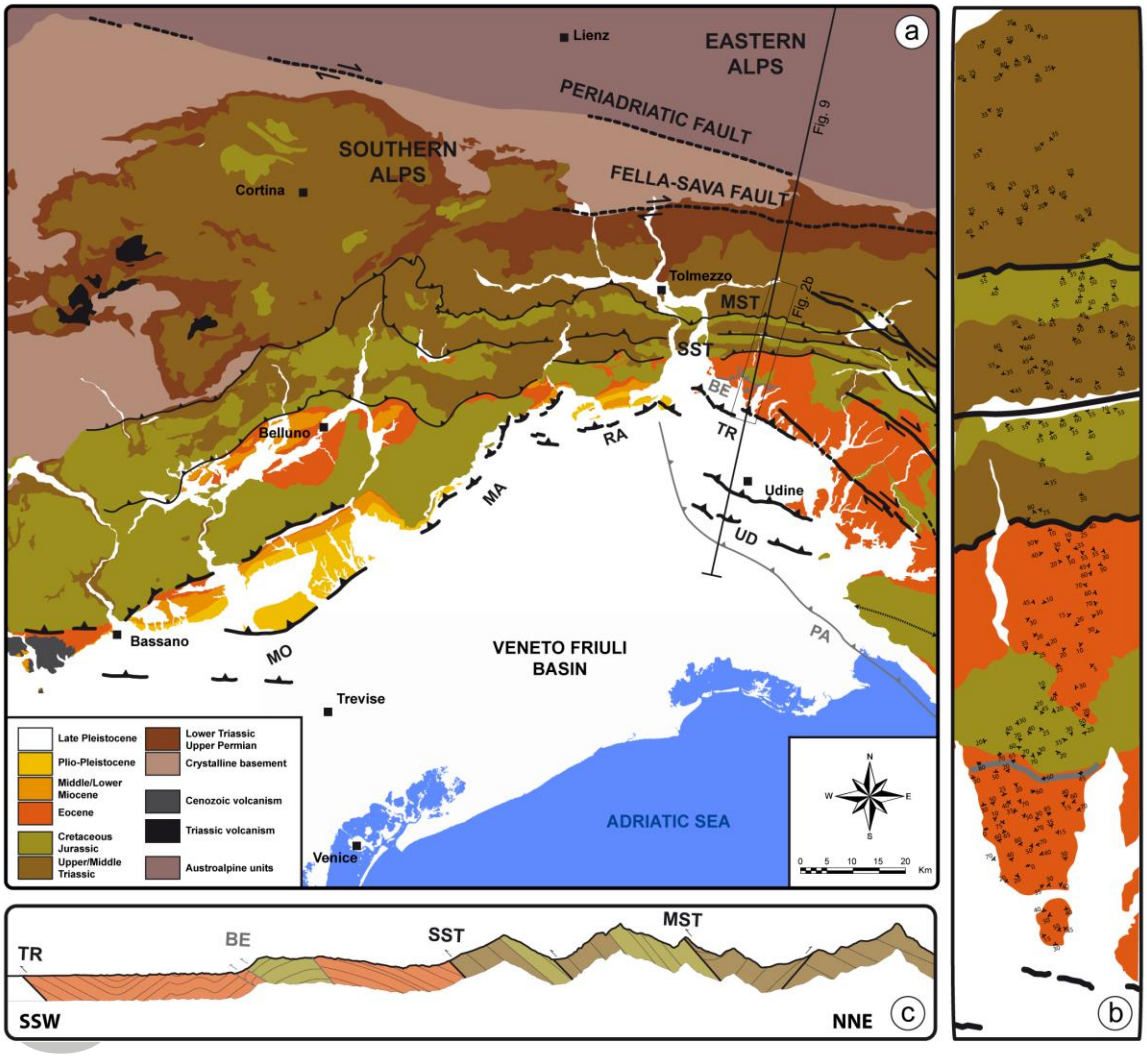

Figure 2: a: Simplified geological map of the eastern Southern Alps after Carulli (2006). Thick black lines represent the active faults (same as in Figure 1), thin black lines the older inactive thrusts, and thin grey lines the inactive Dinaric thrusts. The thick dashed line in the vicinity of Bassano refers to the Bassano Thrust for which no evidence of recent deformation has been identified. b: geological map across a NNE-SSW transect in the eastern part of Figure 2a showing the spots of dip measurements from Zanferrari et al. (2013a). The image is provided in full-resolution in the Supporting Information (Fig. S2) to show the dip values used in constructing the cross-section of Figure 2c. c: Geological section along the area of Figure 2b and according to data of Figure 2b.

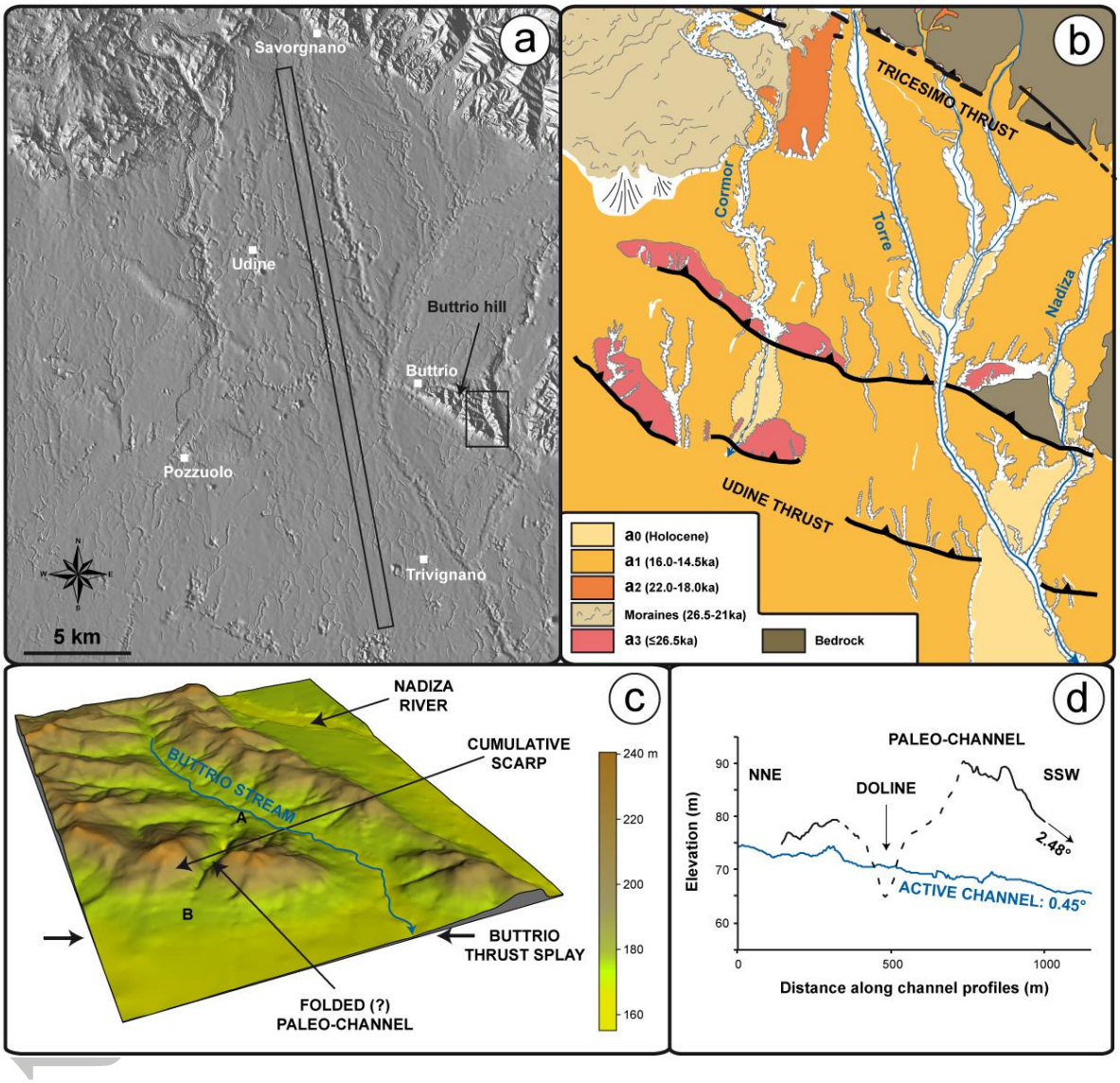

Figure 3: a: 5-m-DEM across the Buttrio and Pozzuolo anticlines derived from 1:5000 topographical maps (1-m-elevation curves and elevation points) provided by the Friuli-Venezia-Giulia region (http://irdat.regione.fvg.it/WebGIS/GISViewer.jsp). The elongated and small rectangular black boxes respectively show the trace of the topographic profiles of Figure 5a and the location of Figure 4c. b: Geomorphic interpretation of the same area. The relative age of alluvial surfaces has been determined from longitudinal profiles, then correlated with the main phases of aggradation of Fontana et al. (2008); age of moraines deposits is from Monegato et al. (2007). c: 3D-view of the Buttrio hill looking NNE. The catchment of a 2-km-long tributary (blue arrow) of the Torre river is visible. A hanging valley (AB segment), parallel to and about 1 km SE of the present tributary outlet, is observed across the cumulative scarp suggesting this is a former outlet of the tributary that has been abandoned and uplifted by thrusting and related folding. d: The topographic profiles of the hanging valley and of the active channel are represented with back and blue lines respectively. The dashed line represents a section of the hanging valley that we interpret as degraded by karstic erosion. Note the apparent tilt (toward the SSW) of the downstream section of the hanging valley with respect to the active channel suggesting it has been folded.

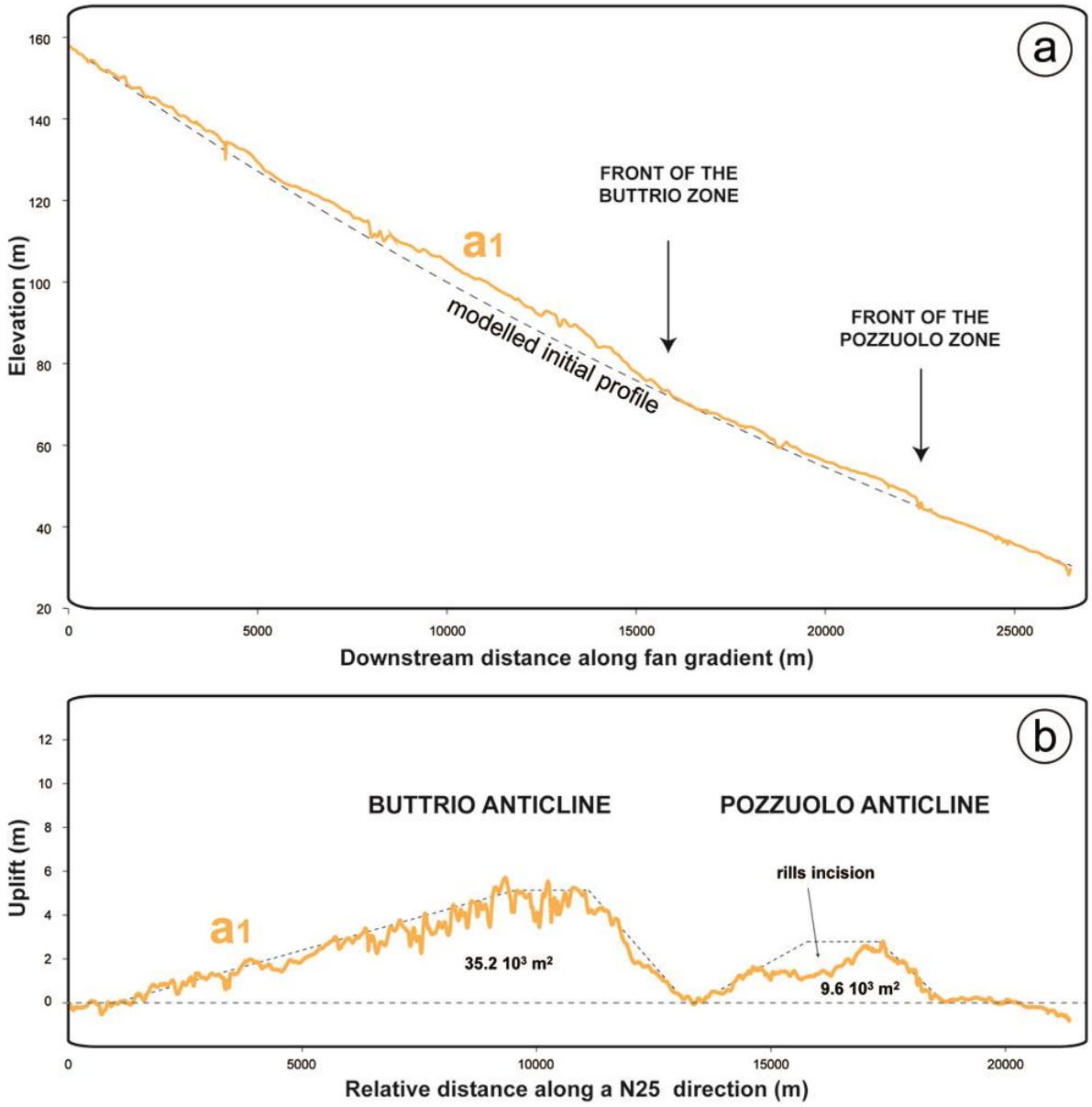

Figure 4: a: A stack of 13 parallel longitudinal profiles along the slope gradient of the a1 fan (see Figure 4 for location) is shown in orange. Two apparently undeformed sections bound intervening topographic bulges upstream and downstream. The dashed line shows the modelled initial profile determined from the two unperturbed sections (see further explanations in the text). b: Uplift profile constructed by computing the difference between observed and modelled topographic profiles. Numbers represent the uplifted cross-sectional area of the Buttrio and Pozzuolo Anticlines.

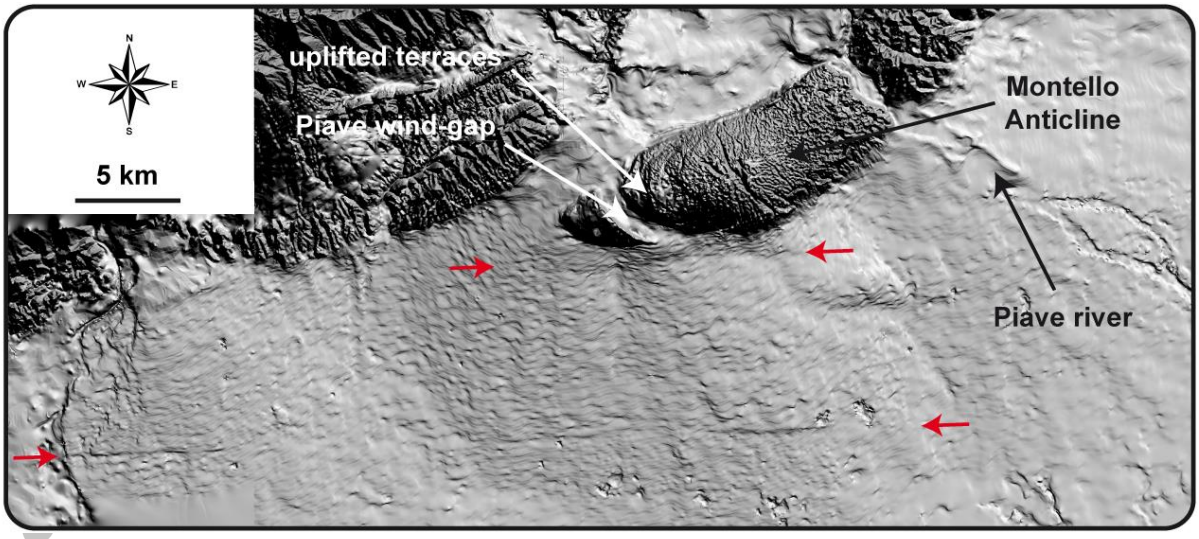

Figure 5: 5-m-DEM derived from 1:5000 topographical maps (1-m-elevation curves and elevation points) provided by the Veneto region (http://idt.regione.veneto.it/app/metacatalog/) and showing the surface expression of the Montello thrust across the alluvial surfaces of the Veneto-Friuli basin. The two sub-parallel E-W-oriented scarps interpreted as the surface expression of two branches of the Montello thrust are shown with red arrows. Note that the Montello anticline, which is associated to the northern branch, bends northward in the E while in the same direction (bottom right corner of the figure) evidence of surface deformation vanishes along the southern branch .

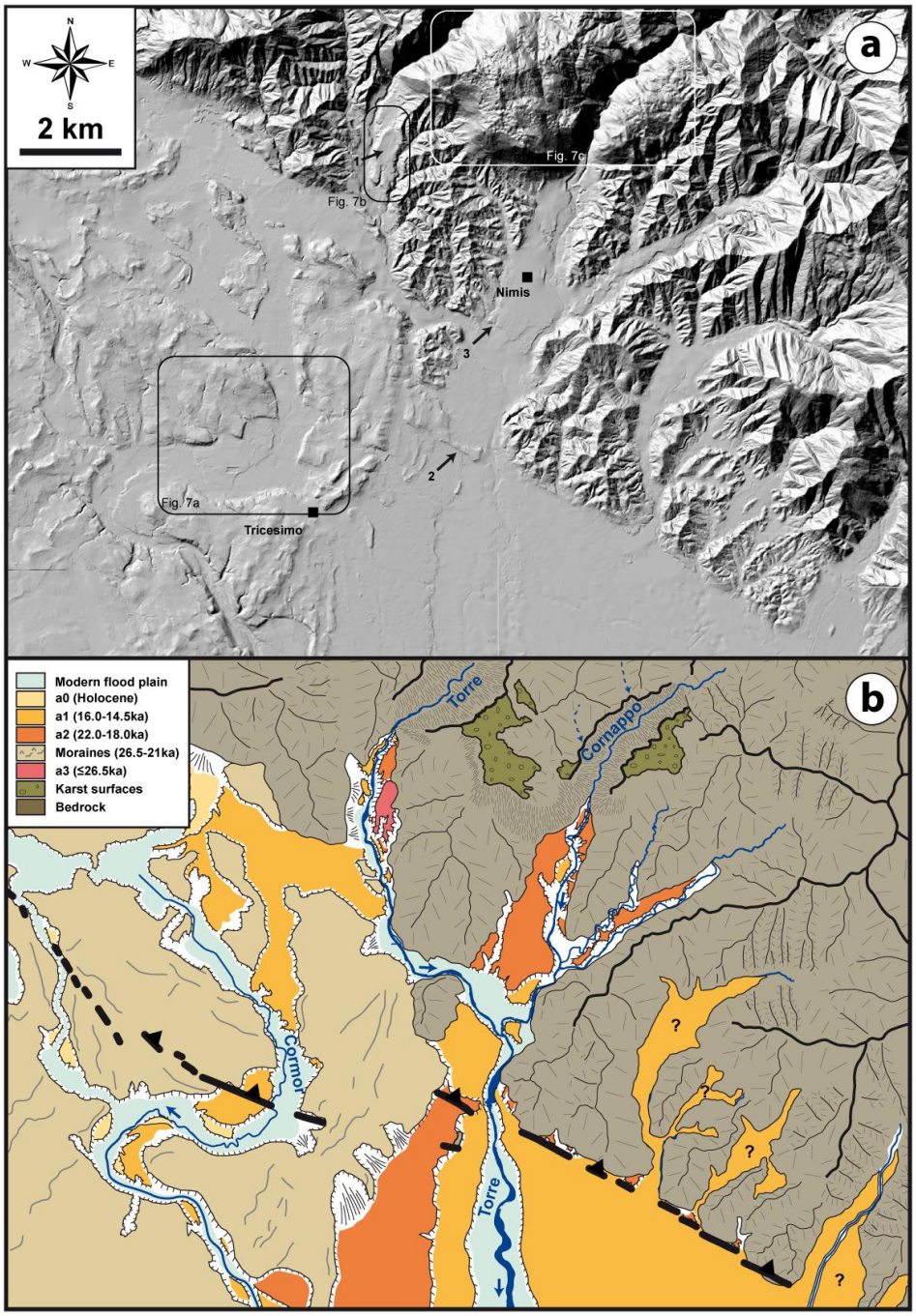

Figure 6: a: 5-m-DEM derived from 1:5000 topographical maps (1-m-elevation curves and elevation points) provided by the Friuli-Venezia-Giulia region (http://irdat.regione.fvg.it/WebGIS/GISViewer.jsp) showing evidence of recent surface deformation associated to the Tricesimo thrust at the front of the eastern Southern Alps. b: geomorphic interpretation of the same area. The black arrows labelled "1", "2" and "3" respectively show the pre-LGM (a3) surface preserved on the left bank of the Torre river, the scarp recorded across the a2 fan and the scarp associated to the front-limb of the Buia anticline. The relative age of alluvial surfaces have been determined from longitudinal profiles then correlated to the main phases of aggradation of Fontana et al. (2008). Note

the preservation of a piece of bedrock above the recent fan deposits, which could be interpreted as a result of uplift above the western branch of the thrust. Dashed blue arrows show the hanging streams on the west side of the Cornappo canyon. Sections of the thrust where surface expression is unclear (western part of the figure) are mapped with dashed thick lines. Question marks refer to alluvial surfaces for which the relative chronology is uncertain.

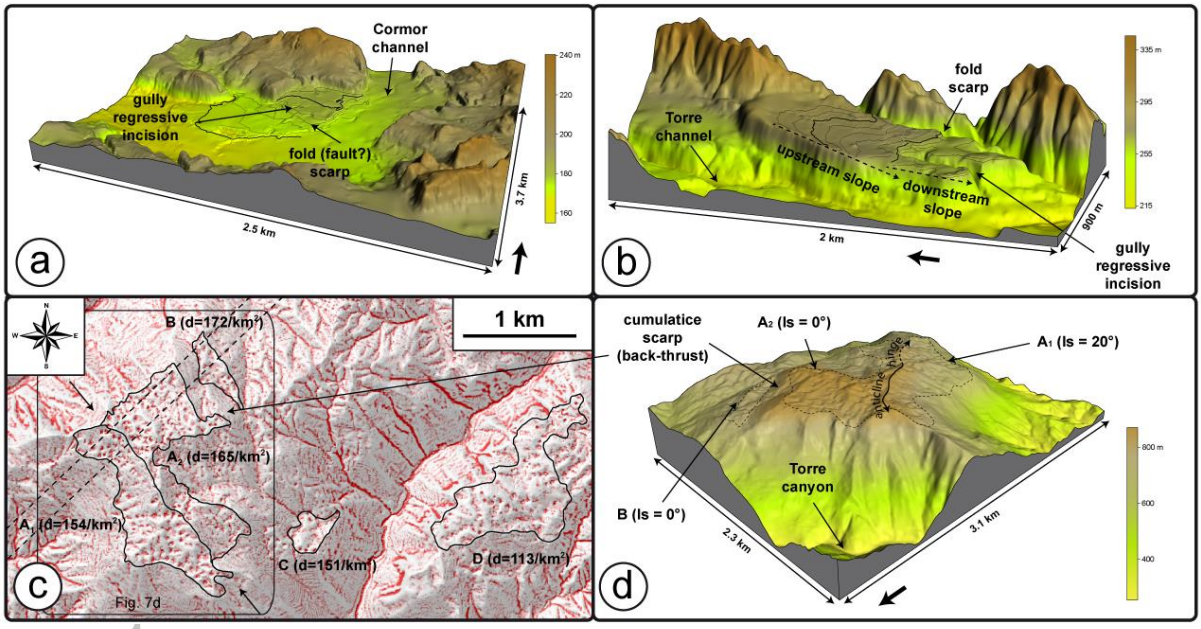

Figure 7: a: 3D-view of the 5-m-DEM (looking NNW) showing the fold (or fault?) scarp across a terrace (a1 tread) of the Cormor river at the front of the Tricesimo Anticline (see Figure 6 for location). Elevation curves are 2 m and are only represented on the alluvial terrace. Thick black arrow points toward the N. b: 3D-view of the 5-m-DEM (looking E) showing the tilt ("downstream slope" versus "upstream slope") of the pre-LGM terrace of the Torre river at the transition from the Bernadia to Buia anticlines (see Figure 6 for location). Elevation curves are 2 m and are only represented on the alluvial terrace. Thick black arrow points toward the N. c: 5-m-DEM of the residual topography (computed from the difference between the 5-m-DEM and a 5-m-DEM smoothed through the low-pass filter of Arcgis) overlied by the shaded relief over the Bernadia anticline (see Figure 6 for location). The areas colour-coded in red represent negative residual topography. Black encircled areas show the four karstic surfaces A (sub-divided into A_1 and A_2), B, C and D. Numbers are dolines density for each individual surface. The two small arrows show the orientation of the slope-break separating A_1 and A_2. Note the consistency of one surface to the other both in terms of aspect and dolines density. The two dashed lines show the area where the 6 profiles of the stack of the Figure 8 have been extracted. d: 3D-view of the 5-m-DEM (looking SE) showing details of the Figure 7c (see Figure 7c for location): topographical scarp between surfaces A_2 and B, and folding (the anticlinal hinge is shown with a double arrow) of the surface A defining the two sub-surfaces A_1 (sloping 20° toward the SE) and A_2 (slope nearly horizontal). ls = local slope. Thin dashed lines encircle the karstified areas (dolines are seen as slight circular depressions). Thick black arrow points toward the N.

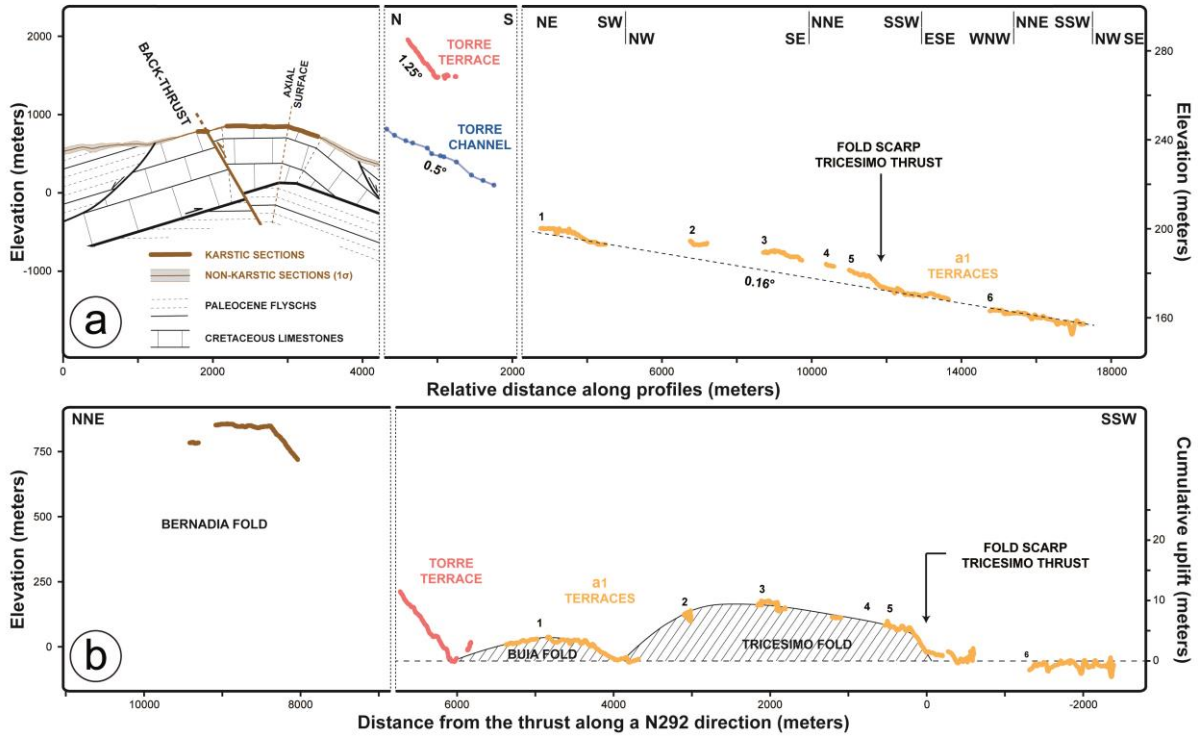

Figure 8: a: The stack of 6 topographic profiles (brown line) across the Bernadia anticline (see Figure 7c for location) is shown with 1σ uncertainty on the left panel. Thick brown lines represent the karstified sections of the profile. The underlying geological structure is modified from Zanferrari et al. (2013a). Note the regular slopes on the karstic sections (the 1σ uncertainty is included in the thickness of the line) and the consistency between the topography of the karstified surfaces and the dips of the geological beds. The middle panel shows the longitudinal profiles of the Torre terrace extracted from the 5-m-DEM and of the Torre channel extracted from elevation points of the 1/5000 topographical map. Note the slope-break in the Torre terrace profile. The longitudinal profile of a1 terraces along the Cormor valley, extracted from the 5-m-DEM is shown on the right panel. Downstream from the observed scarp, it defines a regular 0.16°-slope, which could be considered as the unperturbed a1 topographic gradient. Upstream, a1-topography reveals a clear bulge above the 0.16°-slope (risers labelled 2 to 5) that we interpret as the expression of cumulative folding above the Tricesimo thrust. b: Uplift profiles of the Torre terrace and Cormor terraces have been obtained by cutting the longitudinal profiles of the Figure 8a respectively from the channel slope and from the initial 0.16° unperturbed slope. All profiles have been projected perpendicularly to the Tricesimo Thrust trace to reveal the geometry of the folds. Because no initial undeformed profile is available for the karst surface, its uplift profile is simply represented as a topographic profile (same than in the Figure 8a); for didactic reason the left vertical scale (different than the right one) has then been adjusted to make the Bernadia fold continuous from the Torre terrace to the karstic surface.

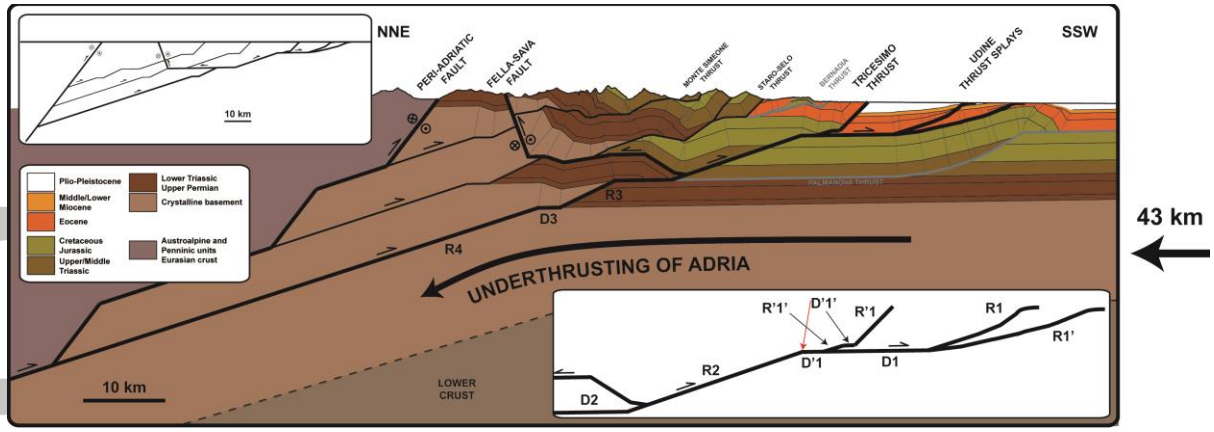

Figure 9 : NNE-SSW-oriented balanced geological cross-section (location shown in Figure 2) without vertical exaggeration constructed by assuming that the Staro-Selo and Monte Simeone Thrusts have a geometry similar to the Tricesimo Thrust. The amount of total shortening on each thrust has then been determined to account for the geometry of the Mesozoic-Cenozoic interface imaged on seismic profiles (Merlini et al., 2002) for the Tricesimo Thrust, and to reproduce the main structures observed at the surface for the Fella-Sava Back-thrust and for the Staro-Selo and Monte Simeone Thrusts. The total shortening on the Udine Thrust Splays, estimated from the displacement of the top of the Eocene sequence (e.g Peruzza et al., 2002; Galadini et al., 2005) is very low (less than 1.5 km) and thus relatively poorly constrained. The grey faults represent structures inherited from the Dinaric NE-SW-oriented compression. The Fella-Sava Back-thrust is assumed to flattens on the main decollement, located along the D2 decollement. How the three main thrusts connect with the Periadriatic Fault at depth is not discussed (question mark) in the present study. Lower right inset depicts the Tricesimo Thrust geometry above the Lower/Middle Trias decollement, with the main fault sections labelled as mentioned in the text. The red arrow shows the axial surface (constrained in the Figure 7), which allows constraining the dip of the R2 ramp. Upper left inset shows the pre-deformation geometry, which implies regular spacing between the three thrusts (thick lines represent the active structures). Note that other minor right-lateral strike-slip faults and back thrusts are observed between the Fella-Sava back-thrust and the Monte Simeone Thrust (Carulli, 2006) but are not represented in the cross-section (nor in the Figure 2) for more clarity and because their geometrical relationships with other structures at depth is difficult to assess (we couldn't conclude whether it is related to the Monte Simeone or to the Staro-Selo thrusts). Bold numbers depict the amounts of total shortening associated to each individual thrust. At depth the Tricesimo thrust has absorbed 12 km, which are distributed at the surface as follows: 10 km along the main Tricesimo thrust, 1 km along the Fella-Sava back-thrust and 1 km along the Udine thrust splays.

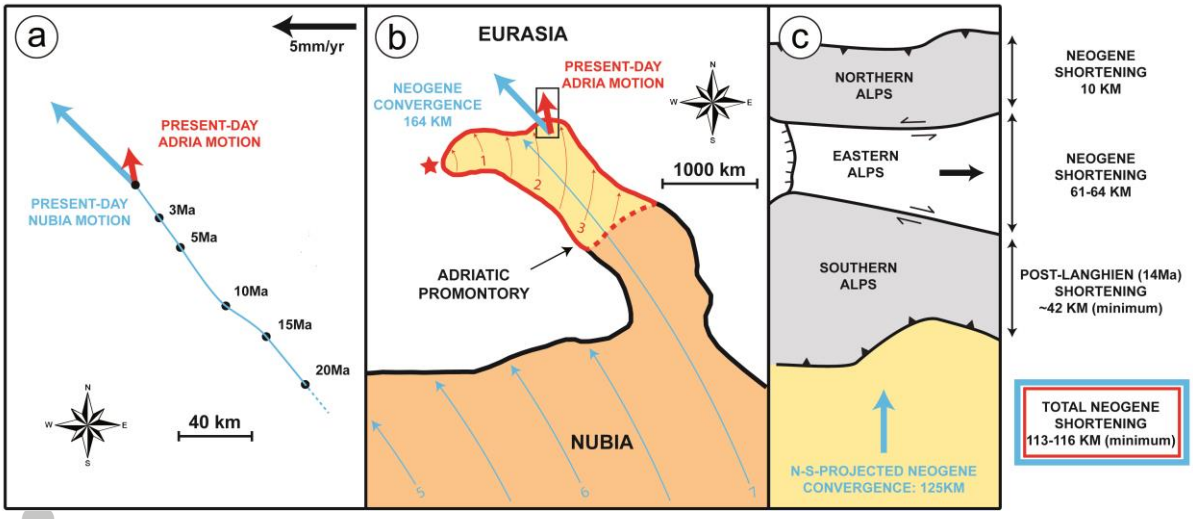

Figure 10: a: Theoretical trajectory (black dots) of a point located in the vicinity of Palmanova over the last 20 Ma based on the reconstructed rotation poles of Nubia (Rosenbaum et al., 2002 and Calais et al., 2003). The theoretical (see the text for additional information) present-day motion of Nubia (blue vector) is from Calais et al. (2003). The present-day motion of Adria (red vector) is from D'Agostino et al. (2008). Note the consistency of the past and present-day motion of Nubia and the clockwise shift observed for the Adria motion. b: Simplified geometry of the long-term plate boundary (thick solid line) between Eurasia (in white) and Nubia (in orange). Boundaries of the Adria microplate is shown with thick (solid and dashed) red lines (the AIH microplate is not represented for clarity). Thin blue and red arrows respectively show the trajectory of the Nubia plate averaged over the Neogene (Rosenbaum et al., 2002) and the present-day rotation of the Adria microplate (D'Agostino et al., 2008) (numbers refer to the corresponding rotation-rates in mm/yr). The red star shows the D'Agostino et al. (2008) Adria rotation pole. Note that the continuation of the blue arrow across the Adria microplate is only didactic and represents the theoretical trajectory of Adria under the assumption that it has always remained rigidly attached to the Nubia plate. According to the same assumption, the expected convergence at the northern tip of the promontory (≈ Palmanova) is represented with a blue vector and accounts for 164 km in a NW-SE direction (Rosenbaum et al., 2002). For comparison, the NNE-SSW direction of convergence according to the Adria rotation pole (D'Agostino et al., 2008) is shown with a red vector (see the text for further information). Black rectangle shows the location of the Figure 10c. c: Simplified tectonic sketch N of the Adriatic promontory at the latitude of Palmanova depicting the three processes accommodating the Neogene Nubia convergence. Shortening assessments (on the right) are from Linzer et al. (2002) and references therein for the Northern and Eastern Alps and this study for the Southern Alps. Estimate for the Eastern Alps is taken at the longitude of Palmanova (Linzer et al., 2002). The value of 42 km of shortening in the Southern Alps comes from the projection of the 43 km (constrained in this paper) along a N-S direction. Lower, the 125-km-vector is the N-S-projection of the 164-km-convergence of Nubia.